University of Denver
Digital Commons @ DU

Electronic Theses and Dissertations | Graduate Studies

1-1-2009

Computational Studies on the Effective Properties of Two-Phase Heterogeneous Media

Elyas El Arbi Tawerghi
University of Denver

Follow this and additional works at: https://digitalcommons.du.edu/etd

 Part of the Computer-Aided Engineering and Design Commons

Recommended Citation

Tawerghi, Elyas El Arbi, "Computational Studies on the Effective Properties of Two-Phase Heterogeneous Media" (2009). *Electronic Theses and Dissertations*. 642.
https://digitalcommons.du.edu/etd/642

This Thesis is brought to you for free and open access by the Graduate Studies at Digital Commons @ DU. It has been accepted for inclusion in Electronic Theses and Dissertations by an authorized administrator of Digital Commons @ DU. For more information, please contact jennifer.cox@du.edu,dig-commons@du.edu.

COMPUTATIONAL STUDIES ON THE EFFECTIVE PROPERTIES OF TWO-PHASE HETEROGENEOUS MEDIA

_____

A Thesis

Presented to

the Faculty of Engineering and Computer Science

University of Denver

_____

In Partial Fulfillment

of the Requirements for the Degree

Master of Science

_____

by

Elyas E. Tawerghi

June 2009

Advisor: Dr. Yun-Bo Yi

©Copyright by Elyas E. Tawerghi 2009

All Rights Reserved

Author: Elyas Tawerghi
Title: COMPUTATIONAL STUDIES ON THE EFFECTIVE PROPERTIES OF TWO PHASE HETEROGENEOUS MEDIA
Advisor: Dr. Yun-Bo Yi
Degree Date: June 2009

ABSTRACT

The effective elastic modulus and conductivity of a two phase material system are investigated computationally using a Monte Carlo scheme. The continuum contains circular, spherical or ellipsoidal inclusions that are either uniformly or randomly embedded in the matrix. The computed results are compared to the applicable effective medium theories. It is found that the random distribution, permeability and particle aspect ratio have non-negligible effects on the effective material properties. For spherical inclusions, the effective medium approximations agree well with the simulation results in general, but the analytical predictions on void or non-spherical inclusions are much less reliable. It is found that the results for overlapping and nonoverlapping inclusions do not differ very much at the same volume fraction. The effect of the particle morphology is also investigated in the context of prolate and oblate ellipsoidal particles.

The geometric percolation thresholds for circular, elliptical, square and triangular disks in the three-dimensional space are determined precisely by Monte Carlo simulations. These geometries represent oblate particles in the limit of zero thickness. The normalized percolation points, which are estimated by extrapolating the data to zero radius, are $\eta c=0.9614\pm0.0005$, 0.8647 ± 0.0006 and 0.7295 ± 0.0006 for circles, squares and equilateral triangles, respectively. These results show that the noncircular shapes and

corner angles in the disk geometry tend to increase the interparticle connectivity and therefore reduce the percolation point. For elliptical plate, the percolation threshold is found to decrease moderately when the aspect ratio ε is between 1 and 1.5 but decrease rapidly for ε greater than 1.5. For the binary dispersion of circular disks with two different radii, ηc is consistently larger than that of equisized plates, with the maximum value located at around r_1/r_2 =0.5.

ACKNOWLEDGEMENTS

First and foremost, I would like to thank my advisor, Dr. Yun-Bo Yi, for all his efforts to provide not only guidance and insight for my research, but also for his support and encouragement as supervisor, teacher, and friend. In addition, I also thank the members of my thesis committee, Dr. Siavash Pourkamli, and Dr. Paul Rullkoetter for their valuable participation and efforts.

Gratefully, I would like to thank Gaddafi International Charity and Development Foundation, namely Dr. Saif Al Islam Muammar Al Gaddafi for their generous support through my graduate studies. Last not least, I appreciate the great learning environment in the School of Engineering and Computer Science, and special thanks to faculty members of department of Mechanical and Material Engineering for the great learning experience.

TABLE OF CONTENTS

Pages

LIST OF TABLES

LIST OF FIGURES

CHAPTER 1 INTRODUCTION

Composite materials exist in almost every aspect in our life from pencils to space stations. Basically, these composites are made of at least two components stiff, strong components embedded in a softer constituent. For illustration, concrete, one of the most widely used building materials in the world, are made of two components, cement and aggregate. The green cement, in fresh or not hardened form, is used as the soft part, matrix, and the aggregate are used as the stiff and strong components. This combination makes it possible to build complex structures.

Heterogeneous materials are designed for many purposes to take advantages of both strength and stiffness of reinforcement materials and light weight of the matrix. Composite materials have witnessed great attention since dawn of Bronze Age. Over the last few decades reinforcement materials have been developed on many levels as the technology advanced and new applications emerged. The differences between mechanical properties of fillers and host materials such as polymer matrix reinforced with filler such as glass fiber, epoxy resin, carbon fiber, or polypropylene, etc are greatly varied. Therefore, Developing appropriate theories and models to predict the effective properties of heterogeneous materials is of utmost importance to design efficient components (Lee, & Paul, 2005).

Material properties can be modeled in three different scales: the continuum macroscopic scale of engineering, the atomic scale, and intermediate mesoscopic scale where microstructure is treated as systematic constituent. One of the widest approaches to define effective properties on mesoscopic scale is effective medium theories (Choy, 1999). Chapter 2 in this work discusses some of these theories in more detail in addition to major mechanical properties of heterogeneous materials.

Modeling and numerical simulation of heterogeneous materials is a growing area especially after the outstanding development in computational tools in terms of processing (number of operations that can computer operate per second) and RAM (Random Access Memory) capacity. However, without super computational power such as multiprocessors, parallel computers, and massive RAM simulation procedures become time consuming and hard to manage. In addition, modeling complex structures can't be accomplished by conventional finite element software. Therefore, the first objective of this work is to develop a new approach to model heterogeneous materials in Chapter 3. Furthermore, effective medium theories were evaluated in comparison to simulation results.

Based on the close relationship between mechanical properties of composite materials and percolation theory, the geometry effect on the percolation thresholds of 2D particles in 3D domain was investigated in Chapter 4. Scaling theories and linear regressions were employed to estimate the percolation thresholds. The simulation results, moreover, are presented and discussed in this chapter. Finally, Chapter 5 highlights the major conclusions that were derived from this work.

CHAPTER 2.1 BACKGROUND AND LITERATURE REVIEW

2.1 Heterogeneous Materials

Nature produces disordered materials, and over the last few decades, it has become obvious that these materials have the optimum structure. Human beings have realized these phenomena, and composites and heterogeneous materials have witnessed widespread applications throughout the history. Even though engineers and materials scientists can employ sophisticated methods to grow pure crystals experimentally, in the real world, they are still dealing with composites and mixture materials. The term heterogeneous materials can be defined as the apparent randomness in the morphology of materials. Topology, the interconnectiveness of its individual elements; and geometry, the shape and size of these individual elements are the main aspects of the morphology (Sahimi, 2003; Choy, 1999).

2.2 Effective Properties of Heterogeneous Materials

The main focus of this work is to understand the effective properties of specific heterogeneous materials and their relevance to both numerical and analytical models. The effective electrical, thermal conductivity and the effective elastic moduli are the predominant properties of interest.

Due to the fact that the mathematical analogy of the formulation of the thermal and electrical conduction in heterogeneous materials is the same, the term effective conductivity refers to both properties in this work (Sahimi, 2003).

2.2.1 The Effective Conductivity

For a two-phase heterogeneous linear materials, g_1 and g_2 are the thermal conductivities for a matrix phase 1 and inclusion phase 2. In steady-state conduction, the governing equation is:

$$\nabla . \mathrm{q}(\mathrm{x}) = 0, \text{ For both phases} \tag{2-1}$$

where q is the local heat flux and the local thermal conductivity in terms of the flux q is defined by the Fourier law,

$$\mathrm{q}(\mathrm{x}) = -\mathrm{q}(\mathrm{x})\nabla\mathrm{T}(\mathrm{x}), \text{ for both phase} \tag{2-2}$$

Where $T(x)$ and $q(x)$ are the local temperature and thermal conductivity at point x respectively.

For a large number of samples,

$$\langle \mathrm{q}(\mathrm{x}) \rangle = -\mathrm{g_e} \langle \nabla\mathrm{T}(\mathrm{x}) \rangle, \tag{2-3}$$

where g_e is effective conductivity tensor.

2.2.2 The Effective Elastic Moduli

In the same manner, for isotropic linear heterogeneous materials consisting of phase 1 and 2 with elastic bulk moduli $K_1$and K_2 and shear modlui μ_1 and μ_2.

$$\nabla.\sigma(x) = 0, \text{ for both phases}$$

where $\boldsymbol{\sigma}(x)$ is the symmetric, local stress tensor

$$\sigma(x) = \lambda(x)tr[\epsilon(x)]U + 2\mu(x)\epsilon(x), \text{ for both phases} \tag{2-4}$$

$$\epsilon(x) = \frac{1}{2}[\nabla u(x) + \nabla\, u(x)^T], \tag{2-5}$$

Here $\epsilon(x)$ is the symmetric, second-rank local strain tensor, $u(x)$ is the local displacement, $\lambda(x)$ and $\mu(x)$ are the local Lame constant, u is the unit dyadic, and superscript T denotes transpose operation on the tensor. And, tr denotes the trace of the tensor.

$$\langle\sigma(x)\rangle = C_e.\langle\epsilon(x)\rangle, \tag{2-6}$$

The effective stiffness tensor C_e can be expressed in terms of only two independent effective elastic moduli K_e and μ_e

$$\langle\sigma(x)\rangle = K_e - 2\frac{\mu_e}{d}\ tr.\langle\epsilon\rangle U + 2\mu_e\langle\epsilon\rangle, \tag{2-7}$$

where d is the dimensionality of the system.

2.3 2D and 3D Material Properties

Young modulus, bulk modulus, shear modulus and Poisson's ratio for a d-dimensional linear isotropic homogeneous materials are specified by $E^{(d)}, K^{(d)}, G^{(d)}$ and $v^{(d)}$. The two-dimensional moduli and the three-dimensional moduli can be connected by making one of the following assumptions either plane-strain or plane-stress elasticity. In the first one, ϵ_{11}=$\epsilon_{12} = \epsilon_{13}$ equal 0, for d=3 (Torquato, 2002).

$$\varepsilon_{ij} = -\frac{v}{E}\tau_{kk}\delta_{ij} + \frac{1+v}{E}\tau_{ij} \tag{2-8}$$

Where $\delta_{ij} = \begin{cases} 1, & i = j \\ 0, & \text{otherwise} \end{cases}$ (The Kroneker delta), i, j= 1,…..d

The previous equation with d=3 can be correlated with d=2 to obtain

$$E^{(2)} = \frac{E^{(3)}}{[1 - v^{(3)}][1 + v^{(3)}]} \tag{2-9}$$

$$v^{(2)} = \frac{v^{(3)}}{1 - v^{(3)}} \tag{2-10}$$

In the same manner, for

$$\tau_{ij} = \lambda\varepsilon_{kk}\delta_{ij} + 2G\varepsilon_{ij}$$

where λ is the lame constant

$$K^{(2)} = K^{(3)} + G^{(3)}/3$$
$$G^{(2)} = G^{(3)} \tag{2-11}$$

In case of plane-stress elasticity, $\sigma_{11} = \sigma_{12} = \sigma_{13} = 0$ in the previous stress and strain tensors expression with d=3 and comparing with d=2 we obtain

$$E^{(2)} = E^{(3)}, \qquad v^{(2)} = v^{(3)}$$

$$K^{(2)} = \frac{9K^{(3)}G^{(3)}}{3K^{(3)} + 4G^{(3)}}$$
$$G^{(2)} = G^{(3)}, \tag{2-12}$$

2.4 Prediction of the Effective Properties of Heterogeneous Materials

Over the past few decades many models have been developed to illustrate the effective properties of heterogeneous materials. Nevertheless, just in the last three decades these models have been developed to incorporate comprehensive structural properties such as the distribution of particles' heterogeneities.

In spite of the fact that the computational power of these days' computers is relatively strong, predicting the exact properties of simple heterogeneous materials is not an easy task to achieve. However, the various properties of composite materials can be estimated by employing efficient computational algorithms and powerful computational tool.

Yet, in order to estimate effective properties of heterogeneous materials, popular effective-medium approximation theories can be employed for this purpose, and the following section describes popular approximation theories and shows their major applications.

2.5 Effective-Medium Approximations

It is well known that the effective medium theories (EMTs) can be used to estimate effective properties of multiphase materials of a wide range of volume fractions (Toroquato, 2002). Wei and Srivastava (2004) applied, for example, one of the basic linear rules of mixing in their work to find properties of carbon nanotube (CNT) polymer composite. In addition, Mondescu and Muthukumar (1999) manipulated EMTs to derive closed form solutions for randomly disturbed particles at low volume fraction. More application will be discussed in the following sections. Since there are many methods used to approximate effective properties of heterogeneous materials, in this work, we focused our research on the most popular theories for spherical inclusions according to Toroquato (2002). The theories that we are going to describe are the Maxwell approximation (Maxwell, 1873), the self-consistent approximation (Gubernatis & Krumbansl, 1975), and the differential effective medium theory (Mclaughlin, 1977).

2.5.1 Effective Conductivity of Multiphase Media

2.5.1.1 Maxwell approximations for spherical inclusion

Maxwell (1873) derived the d-dimensional generalization of the approximation scheme for the case d=3. Figure 2-1 shows a schematic corresponding to Maxwell's

approximation. A sphere of radius $R_o$contained number (N) of smaller spheres of radius R and conductivity σ_2 in a matrix of conductivity σ_2 in d spatial dimensions is shown The volume fraction of the inclusion (small spheres) is $\emptyset_2 = \mathrm{N}(\frac{\mathrm{R}}{R_o})^{\mathrm{d}}$. At r distance larger than R_o, the field E(r) at r distance is the superposition of the field as a result of small sphere, and it can be explained by the following expression.

$$\mathrm{E(r)} = \mathrm{E_0} + \frac{\mathrm{R_o^d}\beta_{21}}{\mathrm{r^d}}[\mathrm{d_{nn}} - \mathrm{I}].\,\mathrm{E_0} \tag{2-13}$$

where $.\mathrm{E_0}$ is a constant intensity field, β_{21} is the polarizability, and n is radial unit normal. Since the intensity field which it produces at a larger distance is

$$\mathrm{E(r)} = \mathrm{E_0} + \frac{\mathrm{R_o^d}\beta_{\mathrm{e1}}}{\mathrm{r^d}}[\mathrm{d_{nn}} - \mathrm{I}].\,\mathrm{E_0} \tag{2-14}$$

$n = r/|r|$ Radial unit normal

$$\beta_{\mathrm{e1}} = \frac{\sigma_{e-}\sigma_1}{\sigma_e + (d-1)\sigma_1} \tag{2-15}$$

By assuming expression $\beta_{\mathrm{e1}} = \emptyset_2\beta_{21}$, we get,

$$\frac{\sigma_e - \sigma_1}{\sigma_e + (d-1)\sigma_1} = \phi_2\left[\frac{\sigma_e - \sigma_1}{\sigma_2 + (d-1)\sigma_1}\right] \tag{2-16}$$

Equation (2-16) defines as Maxwell's approximation of the single-inclusion field. It equals to the lower bound of Hashin-Shtrikman bounds when $\sigma_2 \geq \sigma_1$ and the similar upper bound when $\sigma_2 \leq \sigma_1$.

In the case where $\sigma_2/\sigma_1 = \infty$ (the spheres are superconducting comparative to the matrix).

when $\sigma_2/\sigma_1 = \infty$

$$\frac{\sigma_e}{\sigma_1} = \frac{1 + (d-1)\,\emptyset_2}{1 - \emptyset_2} \tag{2-17}$$

when $\sigma_2/\sigma_1 = 0$

$$\frac{\sigma_e}{\sigma_1} = \frac{(d-1)(d-\emptyset_2)}{d - \emptyset_1} \tag{2-18}$$

For multi phase composite contains M-1 number of different types of spheres with volume fraction $\emptyset_1$……, $\emptyset_M$ the general expression of Maxwell's expression is shown in expression (2-19).

$$\frac{\sigma_e - \sigma_1}{\sigma_e + (d-1)\sigma_1} = \sum_{j=1}^{M} \emptyset_j \left[\frac{\sigma_j - \sigma_1}{\sigma_j + (d-1)\sigma_1}\right] \tag{2-19}$$

2.5.1.2 Self-consistent approximations for spherical inclusion

For M different types of suspensions macroscopic isotropic spherical inclusion with volume fraction $\emptyset_1$……, $\emptyset_M$ and conductivities σ_1……, σ_M, the effective conductivity σ_e by the self-consistency can be described by this formula.

$$\sum_{j=1}^{M} \emptyset_j \frac{\sigma_j - \sigma_e}{\sigma_j + (d-1)\sigma_e} = 0 \tag{2-20}$$

The expression (2-21) shows the self-consistent (SC) approximation for two-phase.

$$\sigma_e = \frac{\alpha + \sqrt{\alpha^2 + 4(d-1)\sigma_1\sigma_2}}{2(d-1)} \tag{2-21}$$

$$\text{With } \alpha = \sigma_1(d\emptyset_1 - 1) + \sigma_2(d\emptyset_2 - 1) \tag{2-22}$$

According to Torquato, (2002) SC approximation may lead to poor prediction of effective conductivity since the theory assumed that the effective properties exist just outside the inclusion phase; moreover, the information about the distribution of inclusion is not included.

In the case of superconducting spherical inclusions in which $\sigma_2/\sigma_1 = \infty$, the effective conductivity is shown in expression (2-23). And in the opposite case, the second phase is insulating spherical inclusions in comparison to phase 1; the effective conductivity can be expressed in formula (2-24).

$$\frac{\sigma_e}{\sigma_1} = \frac{1}{1 - d\emptyset_2} \tag{2-23}$$

$$\frac{\sigma_e}{\sigma_1} = 1 - \frac{\mathrm{d}}{d-1}\emptyset_2 \tag{2-24}$$

2.5.1.3 Differential effective-medium approximations for spherical inclusion

Bruggeman (1935) was the first to introduce the differential effective-medium (DEM). In case of two- phase composite, the phase 1 indicates the matrix phase with volume fraction $\emptyset_1$, and phase 2 indicates the inclusion phase (spherical inclusion) with volume fraction $\emptyset_2$. The differential equation of d-dimensional spherical inclusions can be expressed in the following explicit formula.

$$\sigma_e(\emptyset_2 + \Delta(\emptyset_2) - \sigma_e(\emptyset_2) = \sigma_e(\emptyset_2)\left[\frac{\sigma_2 - \sigma_2(\emptyset_2)}{\sigma_2 + (d-1)\sigma_e}\right]\frac{\Delta\emptyset_2}{1 - \emptyset_2}d \tag{2-25}$$

In the limit $\Delta\emptyset_2 \to 0$, this expression becomes the differential equation

$$(1 - \emptyset_2)\frac{d\sigma_2}{d\emptyset_2} = \sigma_e\left[\frac{\sigma_2 - \sigma_e}{\sigma_2 + (d-1)\sigma_e}\right]d \tag{2-26}$$

By analytical integration with initial condition $\emptyset_2 = 0$

$$\left(\frac{\sigma_2 - \sigma_e}{\sigma_2 - \sigma_2}\right)\left(\frac{\sigma_1}{\sigma_e}\right)^{1/\mathrm{d}} = 1 - \emptyset_2 \tag{2-27}$$

In case of superconducting phase 2, this expression simplifies to:

$$\frac{\sigma_2}{\sigma_1} = \frac{1}{(1 - \emptyset_2)^{\mathrm{d}}}$$

$$\frac{\sigma_2}{\sigma_1} = \infty \tag{2-28}$$

2.5.2 Effective Elastic Moduli of Multiphase Media

2.5.2.1 Maxwell approximations for spherical inclusion

In a similar approach to Maxwell's effective conductivity, Maxwell determined the effective bulk modulus K_e by applying a hydrostatic strain at infinity where $\boldsymbol{\varepsilon}_0 = \varepsilon_0 \mathbf{I}/\mathrm{d}$. The strain field $\varepsilon(\mathrm{r})$ at distance r larger than R_o is defined by the superposition of the field.

$$\varepsilon(\mathrm{r}) = \varepsilon_0 + \frac{\emptyset_2 R_o^{\mathrm{d}} k_{21}}{\mathrm{r}^{\mathrm{d}}} [\mathrm{d}_{\mathrm{nn}} - \mathrm{I}]. \varepsilon_0 \tag{2-29}$$

where k_{21} is the bulk modulus polarizability. The strain at large distance with effective bulk modulus K_e can be expressed as follow

$$\varepsilon(\mathrm{r}) = \varepsilon_0 + \frac{R_o^{\mathrm{d}} k_{e1}}{\mathrm{r}^{\mathrm{d}}} [\mathrm{d}_{\mathrm{nn}} - \mathrm{I}]. \varepsilon_0 \tag{2-30}$$

where,

$$\mathrm{k_{e1}} = \frac{K_e - K_1}{K_e + \frac{2(d-1)}{d} G_1} \tag{2-31}$$

Since $\mathrm{k_{e1}} = \emptyset_2 \mathrm{k_{21}}$

$$\frac{K_e - K_1}{K_e + \frac{2(d-1)}{d} G_1} = \emptyset_2 \left[\frac{K_2 - K_1}{K_2 + \frac{2(d-1)}{d} G_1} \right] \tag{2-32}$$

In term of shear moduli, Maxwell approximation leads to the following expression.

$$\frac{G_e - G_1}{G_e + H_1} = \phi_2 \left[\frac{G_2 - G_1}{G_2 + H_1} \right] \tag{2-33}$$

where K_e is the effective shear moduli of suspensions of identical spheres. G_e and G_1 are the shear moduli of the spherical inclusion and the matrix respectively.

$$H_i \equiv \frac{G_i \left[dK_i / 2 + (d+1)(d-2) G_i / d \right]}{K_i + 2G_i}, \; i = 1,2 \tag{2-34}$$

This method also has special cases in which the spheres are rigid comparing to phase 1 ($\mathrm{G_2 / G_1} = \infty$) as shown in expression (2-35).

$$\frac{G_e}{G_1} = \frac{1 + \frac{d}{2}\,\emptyset_2}{1 - \emptyset_2} \tag{2-35}$$

if $K_1/G_1 = K_2/G_2 = \infty$ both phases are incompressible, and $G_2/G_1 = \infty$

Moreover, when the spheres are holes in incompressible matrix, the Maxwell approximation for this case is shown in expression (2-36).

$$\frac{G_e}{G_1} = \frac{d(1 - \emptyset_2)}{d + 2\emptyset_2} \tag{2-36}$$

The general formula for Maxwell approximation for M-1 different types of spheres with volume fractions and moduli can be described as

$$\frac{G_e - G_1}{G_1 + H_1} = \sum_{j=1}^{M} \emptyset_2 \frac{G_j - G_1}{G_j + H_1} \tag{2-37}$$

2.5.2.2 Self-consistent approximations for spherical inclusion

Similar to the effective conductivity, (SC) approximations were derived firstly by Budiansky (1965) and Hill (1965). For M different types of suspensions macroscopic isotropic spherical inclusion with volume fraction $\emptyset_1$……, $\emptyset_M$, bulk moduli k_1……, k_M, and shear moduli G_1……, G_M the effective elastic shear G_e by the self-consistency can be explicit by this formula.

$$\sum_{j=1}^{M} \emptyset_j \frac{G_j - G_e}{G_j + H_e} = 0 \tag{2-38}$$

where

$$H_e \equiv \frac{G_e\left[dK_e/2 + (d+1)(d-1)G_e/d\right]}{K_e + 2G_e} \tag{2-39}$$

In the case of two incompressible phases in which $K_1/G_1 = K_2/G_2 = \infty$, the expression (2-40) yields to

$$\emptyset_1 \frac{G_e - G_1}{\frac{dG_e}{2} + G_1} + \emptyset_2 \frac{G_e - G_2}{\frac{dG_e}{2} + G_2} = 0 \tag{2-40}$$

In the case were phase 2 is void, and phase 1 assumed to be incompressible then the simple expression of SC approximations in this case is shown in expression (2-41).

$$\frac{G_e}{G_1} = \frac{d\left[(d-1) - (d+1)\phi_2\right]}{d(d-1) - 2\phi_2} \tag{2-41}$$

where $K_2 = G_2 = 0, K_1/G_1 = \infty$,

2.5.2.3 Differential effective-medium approximations for spherical inclusion

In similar approach to (DEM) for effective conductivity, the differential effective medium approximations for bulk or shear moduli K_e, and G_e for two phase composite of d-dimensional spherical inclusions is expressed in formula (2-42).

$$(1-\phi_2)\frac{dG_e}{d\phi_2} = \left[G_j + H_e\right]\frac{G_2 - G_e}{G_2 + H_e} \tag{2-42}$$

and, in the case were phase 2 is perfectly rigid relative to phase 1, the DEM approximations yield to.

$$\frac{G_e}{G_1} = \frac{1}{(1-\emptyset_2)^{\frac{(d+2)}{2}}} \tag{2-43}$$

where $K_1/G_1 = K_2/G_2 = \infty$, and $G_2/G_1 = \infty$.

2.6 Images Processing and Finite Elements Modeling

Over the last few decades there has been a recurrent interest in predicting the effective material properties of advanced heterogeneous composites (Hashine, 1963; Torquato, 1991, 2002; Chen, 2008). The main interest has been focused on the maximum achievability of both elastic modulus and conductivity, by employing either analytical approach or numerical modeling. A number of mechanical, physical and mathematical

principles were employed to derive approximate solutions to estimate the effective properties of heterogeneous material (Hashin, 1983; Chen, 2008).

In addition to analytical approaches described in the previous sections, computational and numerical modeling methods were widely used to investigate the problem, and perhaps the most widespread method is the derived finite element analysis using digital images of 2-D and 3-D composite materials (Garboczi, 1995). This method requires a particular error analysis in deriving the results. An application of this method was explored by Roberts and Garboczi who studied linear elastic properties of random porous composites with various microstructures. However, reduction in local maximum errors, particularly at material boundaries, is not guaranteed. In an alternative approach, there is no need to take x-rays of composite materials to obtain digitalized images which are meshed by using conventional finite element tools. This approach is based on building and simulating composite materials by employing advanced commercial tools to analyze the morphology and properties of composite structures.

In their research, Garboczi and Berryman (2001) applied the same concept to study elastic modui of a material containing composite inclusions in comparison with modified differential effective medium theory (D-EMT). In their modeling method, digital images were used to generate finite element models. Square lattice or cubic pixel images were obtained sporadically to generate the random microstructure, and each square lattice or cubic pixel represents bi-linear or tri-linear element in 2D or 3D respectively. Furthermore, the authors argue that finite element method has to be evaluated in terms of accuracy and reliability since there are no precise analytical data to be compared with the numerical results. Thus, possible sources or errors were evaluated

and considered in their results such as finite size effect, digital resolution, and statistical variation.

The composite inclusion particles were dispersed randomly by random sequential adsorption in which larger particles were placed first in the domain and overlapping is not allowed. Even though the limitation of the D-EMT equations to be compatible to the microstructure of composite, Garboczi et all succeeded to modify this method to match the numerical model. Figure 2-2 shows the D-EMT result for K and G compared to the numerical results for two-size sphere 3D model.

Chen, Jaian, Xu, Limei and Li Hui (2008) recently investigated a direct modeling strategy to predict the effective moduli of composite materials under finite element method. In their work, a numerical model was developed base on the composites of experimental or numerical digital images. These images were processed by Object oriented finite element method (OOF) which is software developed by NIST (National Institute of Standards and Technology, USA) and MIT to generate finite element models. According to NIST, this software was designed to help materials' scientists to calculate macroscopic properties from images of real or simulated microstructures. Figure 2-3 shows an example of a planar specimen constructed with the direct modeling strategy for glass (light shading) and epoxy (dark shading) and a volume fraction of 50-50.

In another work that was conducted by Cai, Tu, and Tao (2005), a more modern method doesn't involve digital imaging was implemented to model what was called "the optimal design of physical properties" of polytetrafluoroethylene or (PTFE) composites with random 3-D inclusion. This model was used to investigate thermal conductivity of PTFE composites. However, their model was limited to the composites of unidirectional

fibers. The main objective of their work was to study the thermal conductivity of PTFE composites reinforce with single-phase and two phase reinforcement. Figure 2-4 shows 3-D FE model of two phase reinforcement, and figure 2-5 shows 3-D FE model of one-phase reinforcement. Moreover, a comparison between finite elements results and experimental values are shown on figure 2-6 and it shows good agreement between both values.

Modeling two-phase composite contains symmetrical randomly distributed particles without using digitalization imaging takes a lot of effort to achieve by any means. However, modeling inclusions with no axes of symmetry such as fibers and ellipsoids is a more challenging task. Lee and Paul (2005) developed an analytical model for composites containing three-dimensional ellipsoidal inclusions; however, their model is limited for unidirectional aligned inclusions. This limitation makes it possible to employ Eshelby's equivalent tensor with a Mori-Tanaka model. Figure 2-6 shows a schematic of a three dimensional ellipsoidal inclusion and its radii a_1, a_2, a_3. The elements of the model are shown on figure 2-7 which consists of two constituent the oriented ellipsoidal inclusions and the infinite elastic matrix.

2.7 Percolation and Effective Properties

Percolation threshold of composite materials has a significant effect on the behavior of effective properties. Near percolation threshold, the behavior of effective transport and elastic properties of materials is unlike those for pure materials. Extensive

mathematical and numerical models have been developed to understand this phenomena and its effect on materials properties. In foremost recent work, for example, Yi and Sastry (2002) derived an analytical approximation of 2-D and 3-D dimensional percolation threshold for fields of overlapping ellipses. Yi (2006) also studied the void percolation problem of a medium containing overlapping ellipsoids. These results are useful in predicting the minimum amount of material needed to achieve conductivity or mechanical strength. In addition to the predictions of percolation threshold, the elastic modulus and conductivity of fibrous (Berhan et al., 2004; Zhang, & Yi, 2008) or particulate systems (Wang, Yi, & Sastry, 2004) were also studied computationally. Chapter 4 provides literature review regards percolation and its application in addition to the second objective of this work.

2.8 Universal Scaling Laws for Percolation quantities

The microscopic details of a system affect the numerical value of any percolation quantity; however, near percolation threshold p_c most percolation quantities follow scaling laws in which the network structure and its microscopic details have insignificant effect (Sahimi, 1994). This low is applicable for many of percolation quantities such:

1. Percolation probability P (p), this is the probability that, when the fraction of occupied bonds is p, a given site belongs to the infinite cluster of occupied bonds.

   $P(p) \sim (p - p_c)^{\beta_p}$

2. Correlation length $\xi_p(p)$, for $p<p_c$, this is the typical radius of the connected clusters, and the length scale is macroscopically homogeneous. For $p>p_c$, L, system's linear size, must be larger than the correlation length for the result of any Monte Carlo simulation to be independent of L.

$$\xi_p(p) \sim (p - p_c)^{-v_p}$$

3. Effective electrical conductivity g_e , this is the electrical conductivity of a random resistor network in which a fraction p of bonds is conducting and the rest are insulating.

$$g_e \sim (p - p_c)^{\mu}$$

4. Effective elastic modului G. G can be defined as the elastic modui of the network in which a fraction p of the bonds are elastic elements and the rest are soft or voids elements.

$$G \sim (p - p_c)^{f}$$

The topological exponents β_p and v_p are totally universal, and they depend on the dimensionality of the system and indecent of the microscopic structure. The same case for the transport exponent μ andf; however, in some cases this condition may be violated.

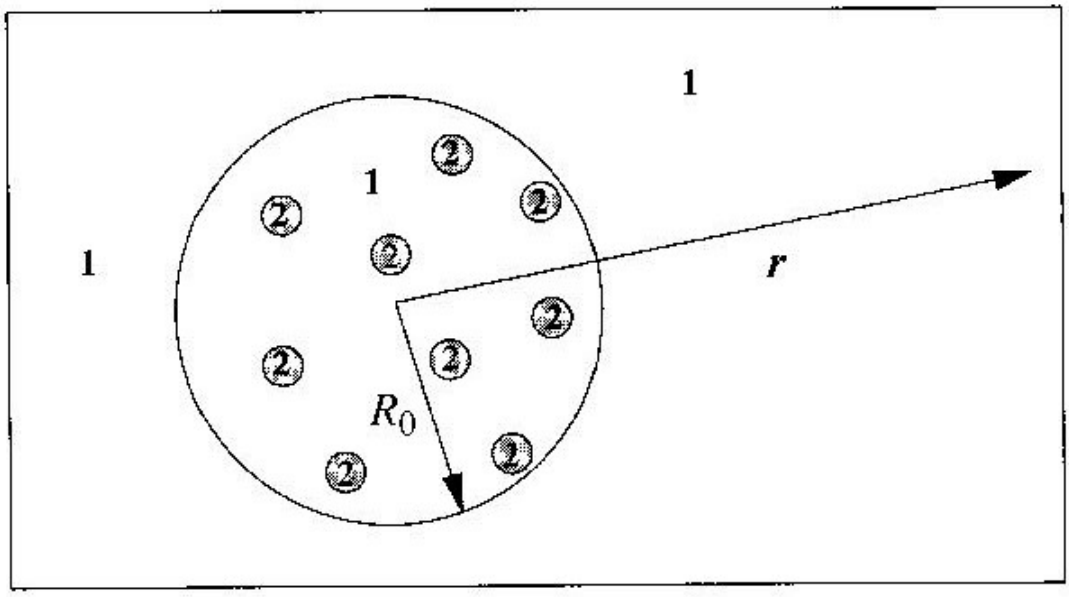

Figure 2-1 A schematic corresponding to Maxwell's approximation. A composite sphere of radius R_o , composed of spherical particles (phase 2) in a matrix (phase 1), is immersed in an infinite matrix of phase 1.

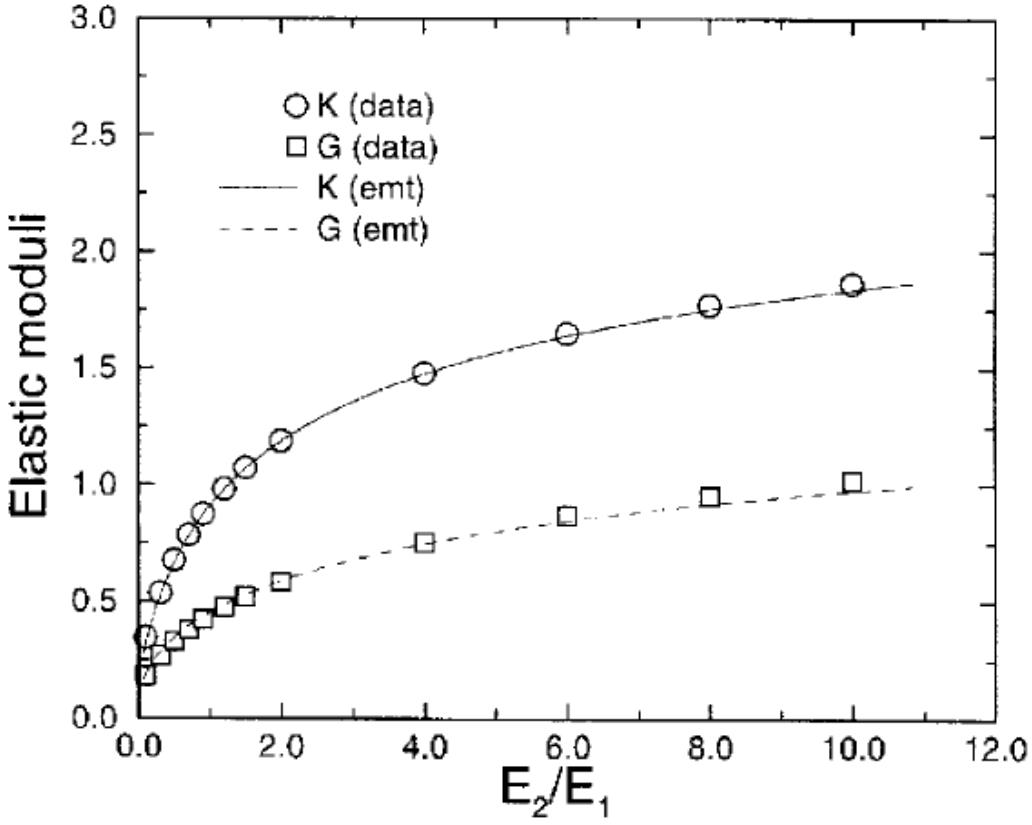

Figure 2-2 The D-EMT results for K and G compared to the numerical results for the two-phase 3D model.

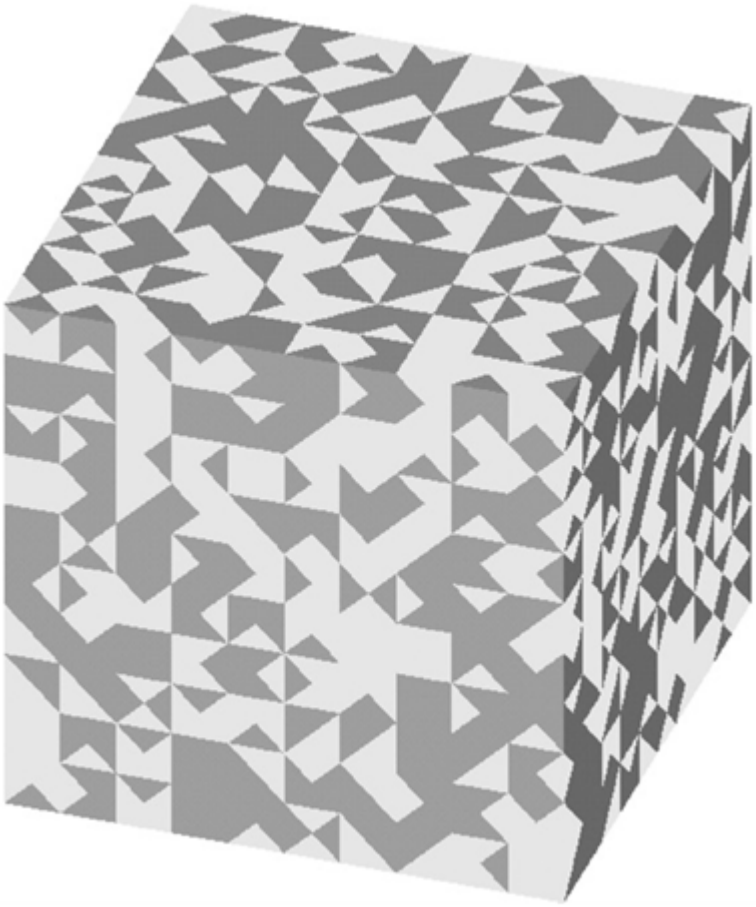

Figure 2-3 An example of a planar specimen constructed with the direct modeling strategy for glass (light shading) and epoxy (dark shading) and a volume fraction of 50-50.

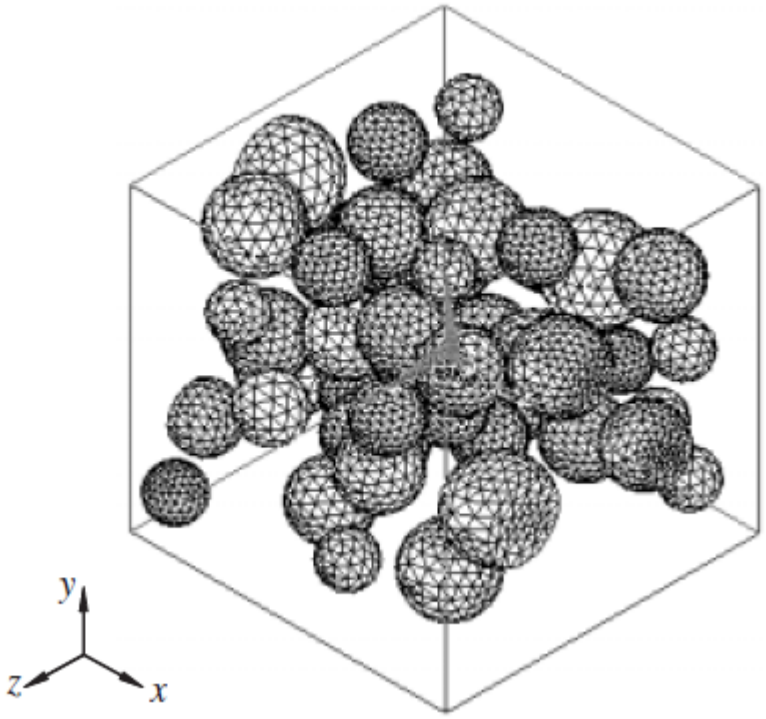

Figure 2-4 A 3-D FE model of two phase reinforcement

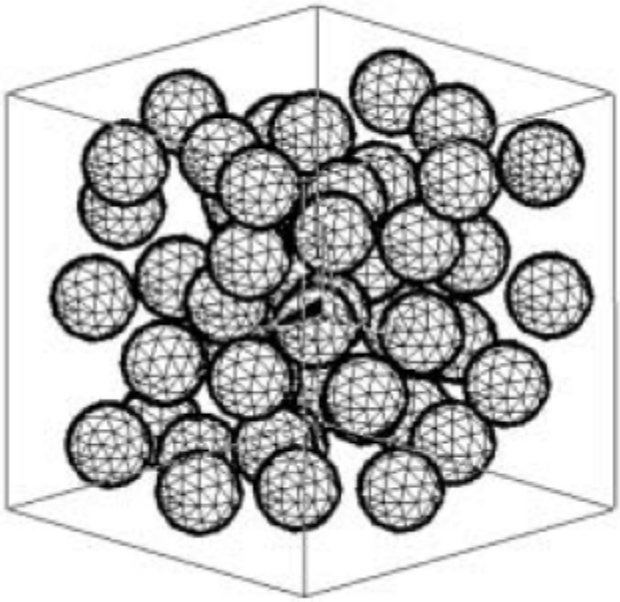

Figure 2-5 A 3-D FE model of one-phase reinforcement.

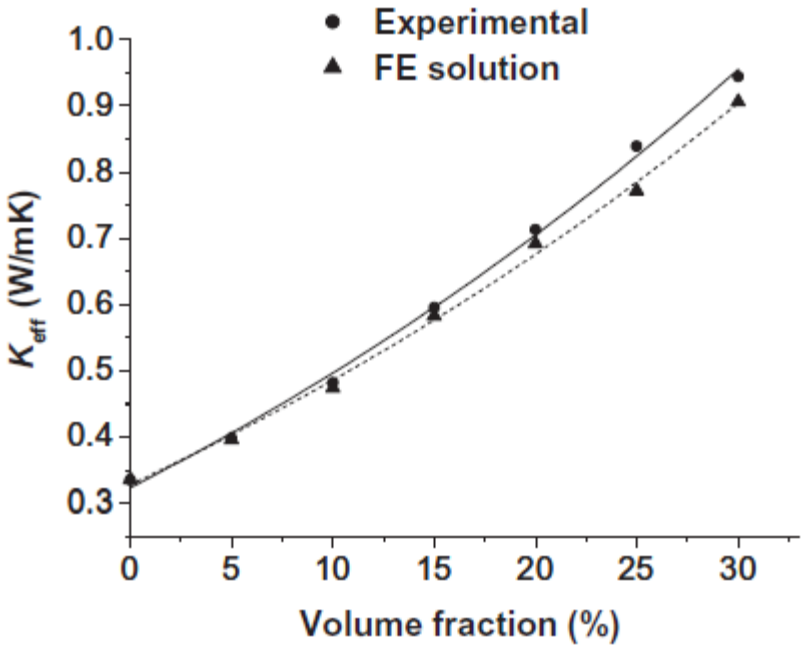

Figure 2-6 A comparison of FE results and experimental values

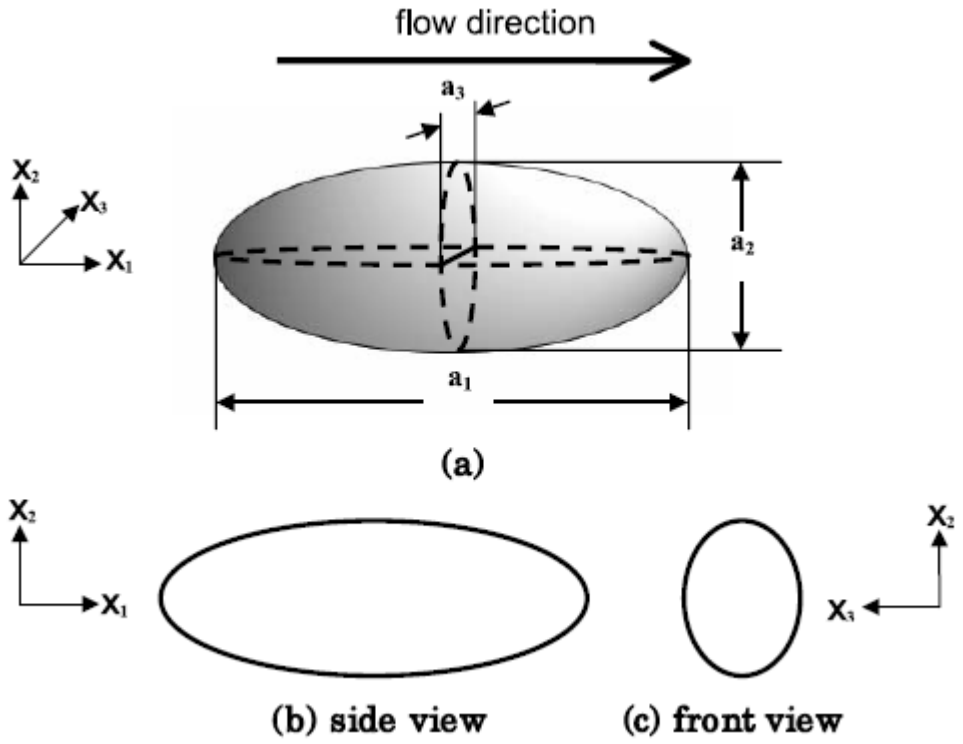

Figure 2-7 Schematic views of a three dimensional ellipsoidal inclusion, along with its side and front view.

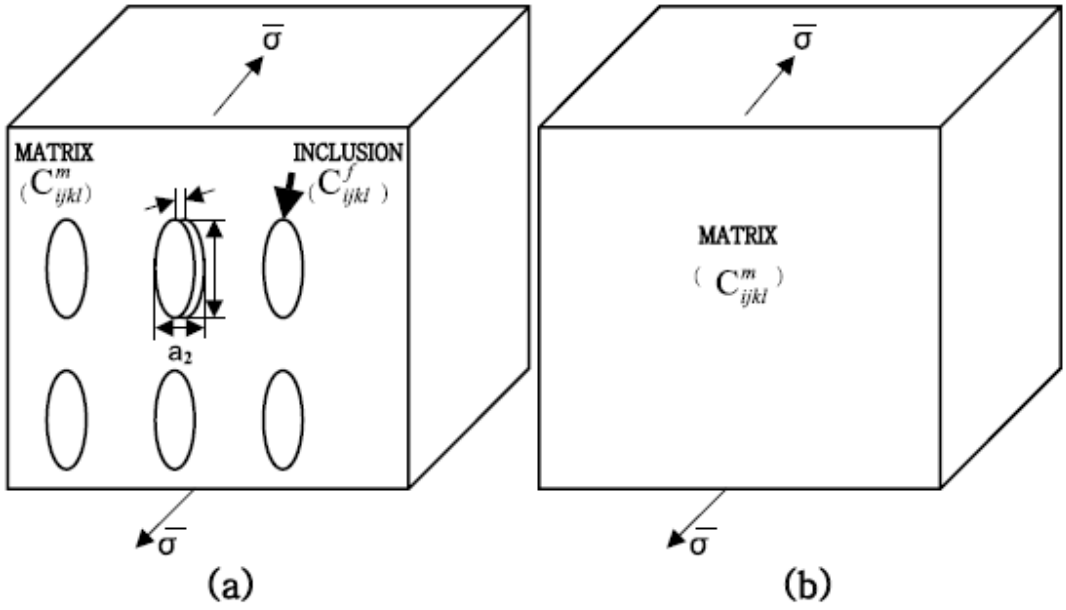

Figure 2-8 A composite formed from aligned ellipsoidal inclusion with aspect ratio of two.

CHAPTER 3 EFFECTIVE PROPERTIES OF TWO-PHASE HETEROGENEOUS MEDIA

Dealing with the finite element modeling of a multiphase material system is not in the slightest an easy task since the inclusion materials are interconnected with the matrix. The persistent obstacles to mesh automation of complex structures are well known and no individual commercial code is capable of handling the problem of interest. In the current work, a new, direct simulation method that does not rely on digitization of the material phase was employed, thus allowing more accurate modeling of the interconnected structures. The method is based on the Direct Delaunay tessellation scheme, i.e. a general triangulation method from scattered points. Several commercial codes worked jointly in the model development: Matlab® (2005), Comsol Multiphysics® (2006) and Abaqus® (2006) as well as a standalone code written in C programming language for particle dispersion. The analytical approximations have also been obtained from the effective medium theories for both validation and comparison purposes.

For realistic multiphase composites, the interfacial effect could play an important role. For example, Torquato and Rintoul (1995) developed rigorous bounds on effective conductivity for the interfacial surface effect between spherical inclusions and matrix, and this work was later extended for other problems as well (Miloh, & Benvensite, 1999;

Benvensite, 2006).In addition, the mechanical contact problems were also investigated in the context of random media recently (Yi, 2008).

3.1 Methodology

3.1.1 Two Dimensional Computational Models

Matlab® and Comsol® were directly used to create finite element models in a unit size rectangular domain required for the subsequent mechanical analysis. In particular, a dynamic collision algorithm was applied to randomly deploy nonoverlapping voids or fillers. The material properties, meshing and analysis procedure were conducted using the graphic user interface of the program of interest.

Three different cases were investigated as follows: Case 1 Arrays of circular voids were uniformly dispersed in the matrix with the same spacing in both x- and y-directions. The voids had the same size with a fixed radius of 0.05 (normalized unit). Figure 3-1 (a) shows the meshed model, which was generated via the built in optimized mesh quality in Comsol ®, and number of triangular elements in the model was 6800. In the second case, the circular voids were randomly distributed in the domain. “Random” here is referred to as a Poisson process following a uniform probability density. Figure 3-1 (b) shows an example of randomly distributed circular voids with 7447 elements. In the

last case, the circular voids in Case 2 were replaced by disk-shaped circular fillers, and therefore two dissimilar materials were involved in this case.

3.1.2 Boundary Condition and Analysis Parameters

A prescribed displacement of 0.01 was applied along the y-direction, and an isotropic linear elastic analysis was performed to determine the reaction forces. The effective elastic modulus of the system was estimated by taking the ratio of the resulting stress to the preset strain. According to the scaling theories, the result computed in this way is a function of the simulation domain. However, when the ratio of the domain size to the size of inclusions is sufficiently large, the result will approach the asymptotic limit. Several physical assumptions and mathematical simplifications were made: (1) for circular fillers, the two phases had the same Poisson's ratio (0.3) in order to minimize the number of variables in the model; (2) The interfaces between dissimilar materials were bonded by either adhesives or special chemical or thermal treatment; therefore, no contact surfaces were modeled; (3) The simulation results were normalized against the properties of the matrix, and hence the modulus or conductivity was dimensionless.

3.1.3. Three-Dimensional Computational Models

In the 3-D simulations, a different scheme was implemented to automate the modeling process due to the difficulties in a direct simulation using the commercial software. The procedures involve a three-step procedure: first, a similar collision algorithm was employed to generate overlapping or nonoverlapping inclusions. Second, the obtained geometric data was used to generate a finite element mesh by a standard

Delaunay Tessellation scheme. In the last step, the output data of the code bundle was written into a script file readable by ABAQUS® for the subsequent finite element analysis.

Three different models were investigated: (1) overlapping spherical inclusions, (2) nonoverlapping spherical inclusions, and (3) nonoverlapping ellipsoidal inclusions. Since the problem involving void inclusions was already studied in the 2-D cases, here our attention was focused on the continuum problems and the inclusions in all three models were assumed to be fillers.

In the first model, all the spheres were identical and had a radius of 0.1 (the simulation domain remains as a unit cell). These spheres were deployed randomly in the matrix following an algorithm similar to the one used in the 2-D models. The tetrahedron finite element mesh was generated via a 3-D Delaunay tessellation scheme in Matlab®. The volume fraction of spheres was obtained by summing the volume of each individual element that was located in the interior of at least one of the spheres. Figures 3-2 (a) and (b) show models of the mid-plane cross sections of overlapping spheres. The last step is meshing procedures. The mesh information was exported to an ABAQUS® input file.

In addition to mechanical analysis, the effective conductivity of the material system was also evaluated by a steady state heat transfer analysis. More specifically, unit temperature difference was applied on two opposite sides of the unit cell and the reactive heat flux was computed. The total heat transfer rate by summing the nodal heat flux is the effective conductivity of the system. Regardless of the physical distinction between thermal and electrical conduction, the normalized result can be interpreted as either the

thermal conductivity or electrical conductivity because of the mathematical analogy between the two phenomena.

Nonoverlapping spheres were modeled in a strategy similar to that for nonoverlapping circular disks except that the process was more computationally intensive. Figure 3-3 (a) shows a computer-generated system of nonoverlapping random spheres.

In addition to spherical inclusions, a specific model was developed to model ellipsoidal inclusions. Two types of ellipsoidal particles, oblate (disk-shaped) and prolate (cigar-shaped) were modeled and investigated. Figure 3-3 (b) shows a computer-generated random system of oblate ellipsoidal particles. All the ellipsoids were assumed to be impermeable. The locations and geometric data of ellipsoidal particles were generated in the same way as that used for spherical particles. Although a generalized ellipsoid would be a tri-axial particle, here we focused on ellipsoids of revolution only. As a result, only two parameters were needed to determine the geometric shape of each particle: namely, minor axis length and major axis length. To generate random ellipsoidal particles, the center point locations were distributed randomly, and the Euler angles of the axes also followed the appropriate density functions of probability.

3.2 Simulation Results and Discussion

3.2.1 Circular Inclusions

First of all, the effect of circular voids on effective elastic modulus of circular voids was investigated. Figure 3-4 shows a plot of the simulated elastic modulus obtained from the finite element analysis for the following two cases: (1) uniformly distributed circular voids and case (2) randomly distributed circular voids. It can be seen that the effective elastic modulus decreases with the void volume fraction in both cases. In addition, the modulus of the material containing uniformly distributed circular voids is greater than that of the material containing randomly distributed voids. In the second case, the reason could be the effect of the higher stress concentration in the regions where the voids are located very close to each other. In the same figure, the simulation result is also compared to the effective medium theories including the Maxwell approximation and the SC approximation. Even though the assumption here is that the matrix is assumed to be incompressible, the Maxwell approximation shows a similar pattern to uniformly distributed voids. The SC approximation also shows agreement with the simulations for both uniform and random distributions at lower volume fractions. However, there is a significant discrepancy at higher volume fractions. Overall, the simulation results roughly fall between the Maxwell approximation and the SC approximation results.

To investigate the effect of a two phase material system, the void spaces in the previous model were replaced by elastic circular disks in figure 3-5 (a), where the results are shown for the effective elastic modulus of a plate containing randomly distributed

disks. A comparison has been made between the simulations and those predicted by the linear rules of mixing. In parts (a), (b) and (c) of figure 3-5, the normalized modulus of the inclusions varies from 2, 5 to 7, respectively, whereas the normalized modulus of the matrix material is fixed to the unit value. It can be seen that the simulation results fall between the upper and lower limits of linear rules of mixing. In addition, the difference between the upper and lower limits increases with the modulus of the disks. Apparently, the effective modulus of the composite material increases with both the volume fraction and the modulus of the embedded particles. For example, the effective moduli (E_{eff}) increases by 40% at 50% volume fraction of disks with $E_2/E_1=2$. At the same volume fraction, E_{eff} increases by 100 % and 130 % for $E_2/E_2=5$ and 7, respectively. Similar results have also been obtained for uniformly distributed disk-like inclusions.

Figure 3-6 (a) shows the comparison between the finite element simulation and the effective medium theories. The simulation models along with all the assumptions remain the same as those used in figure 3-5. It is seen that the effective modulus of the system falls between the Maxwell and the SC approximations. In figure 3-6 (a) where $E_2/E_2=2$, an excellent agreement can be seen between the results for the entire range of volume fraction. Using either of the approximation theories would yield an error less than 2% in the predicted elastic modulus. In figures.3-6 (b) and (c) where $E_2/E_2=5$ and 7, respectively, the simulation result shows good agreement with the approximation theories at a volume fraction below 40%. At a volume fraction above 40%, the results deviate slightly from the approximation theories. Nevertheless, the Maxwell theory and the SC

approximation consistently provide a lower and an upper bound for the simulation results, respectively.

3.2.2 Spherical Inclusions

The above work was extended to the three-dimensional case in which the matrix contains randomly distributed spherical particles instead of circular disks. Figure 3-7 shows a comparison of the elastic modulus between the simulation and the approximation theories. The spheres are allowed to overlap in this case and $E_2/E_2=4$ is assumed. The Poisson's ratio is fixed to 0.23 in both phases. It can be seen that the simulation results fall between the Maxwell and the SC approximation theories. Apparently, the effective modulus increases with the sphere volume fraction. Also, it has been noticed that the SC approximation generally yields much better results than the Maxwell approximation.

In addition to the mechanical analysis, we also performed the conductivity analysis for overlapping spheres as shown in figure 3-8. The dimensionless conductivity of the matrix material and the conductivity of the spherical inclusions are assumed to be 1 and 4, respectively. The simulation results are compared to the three different effective medium solutions: Maxwell, SC and DEM. It is seen that the effective conductivity increases with the sphere volume fraction according to a power-law form similar to the elastic modulus. All three approximations agree very well at lower volume fractions, especially below 20%. However, differences among FEM, DEM and Maxwell can clearly

be seen at higher volume fractions. In comparison with the simulation results, the SC solution once again presents the best solution among the three approximation methods.

The above work was further extended to nonoverlapping spherical inclusions, which are believed to represent more realistic material systems. The predicted effective elasticity modulus and conductivity are shown in figures 3-9 and 3-10 respectively. In the case of mechanical analysis, figures 3-9 (a), (b) and (c) show the effective elastic modulus for three cases where E_2/E_2=2, 4 and 0.25 respectively. In figure 3-9 (a), it can be seen that the simulation results are in excellent agreement with the approximations. In figure 3-9 (b), the difference is discernable, but not quite significant. At lower volume fractions, the SC solution is closer to the simulation results whereas at the higher volume fraction the Maxwell approximation tends to be closer. This is somewhat different from the results of overlapping particles. A comparison of figure 3-7 and figure 3-9 (b) shows that the effective modulus does not differ significantly between the overlapping and nonoverlapping inclusions. In figure 3-9 (c), E_{eff} decreases with the sphere volume fraction since the spheres are “softer” than the matrix in this case. The comparisons between the EMTs and the simulations generally do not show good agreement here, particularly at higher volume fractions. For example, when the sphere volume fraction is 50%, the simulation, the Maxwell solution, and the SC solution predict results of 2.3, 2.0 and 2.1, respectively. One reason for that could be related to the limitation of the approximation theories for predicting the effective moduli of composite materials.

The corresponding conductivity analysis was also performed on nonoverlapping spheres as shown in figure 3-10. Again, we chose the ratio of the conductivities of the

matrix and the spheres to be 1:4 for consistency. Clearly, the simulation results fall between the SC solution and the DEM solution while the Maxwell solution underestimates the conductivity. The effective conductivity increases nonlinearly as the sphere volume fraction increases. For example, at 60% volume fraction, the effective conductivity increases by approximately 150%. In addition, by comparing figure 3-8 and figure 3-11, it was found that the conductivity does not differ very much between the overlapping and nonoverlapping conditions.

3.2.3 Ellipsoidal inclusions

As mentioned previously in the method section, two types of ellipsoidal particles, namely Oblate and Prolate, were investigated in this work, and the outcomes of these simulations were compared to the EMTs. Figure 3-12 shows the mechanical analysis of two-phase composite containing nonoverlapping ellipsoidal inclusions which is either oblate or prolate. The aspect ratio for both types of ellipsoids is 1.4. Again, the correlation is excellent between the simulations and the analytical predictions. The Maxwell approximation exhibits close correlations to both types of ellipsoidal particles at volume fractions below 20%. It has also been noticed that the results of the prolate particles and oblate particles are nearly the same at lower volume fractions, yet they start to deviate from each other at a volume fraction above 40%. This deviation increases with the volume fraction, and it is expected that at the closed-packing limit, there should be an appreciable difference between the two cases. In the conductivity analysis as shown in figure 3-13, it is again seen that the SC approximation provides a better prediction of the

results compared to other theories. In addition, the composite containing prolate particles have a higher conductivity than those containing oblate particles although the difference is less than 5% at a volume fraction below 60%.

The effect of aspect ratio on the effective elastic modulus is presented in figures 3-14 (a) and (b). The "aspect ratio",ε is defined as the ratio of the major axis length to the minor axis length. The geometry is assumed to be a prolate ellipsoid of revolution, and hence the two minor axes have the same length. The number of ellipsoids used in the simulation varies from 170 to 1,020 depending on the volume fraction of particles. From the figure, it is seen that the effective modulus of the composite is a function of the particle aspect ratio. In figure3-14 (a), the mean radius of particles is 0.1, and it is seen that the maximum modulus of ellipsoidal particle system is 5% higher than that of spheres at the same volume fraction. In figure 3-14 (b) where the mean radius of particles is 0.05 and at the same volume fraction, the maximum value of the modulus is approximately 10% higher than that of a spherical particle system. Although none of the effective medium solutions agrees with the simulations, the SC approximation yields a closer result. More interestingly, evidence shows that the relationship between the modulus and the aspect ratio is not monotonic. Rather, the result oscillates when the aspect ratio varies. More specifically, the effective modulus decreases in the range ε=1~2, and then increases for ε=2~4. The maximum value occurs at ε=4, and then it decreases again. Further increase of the aspect ratio leads to only a mild change of the result: from figure 3-14, it can be seen that the moduli for ε=4 and 10 are not far away from each other. It is conjectured that the spatial distribution of the stress concentration

zones may play a role in this oscillatory result, but the exact reason behind the phenomenon is not clear yet.

Finally, it should be pointed out that for a general two-phase elastic material system involving four distinct parameters (E_1, ν_1, E_2, ν_2), Dundurs, (1969) proved that the stress field can be written in terms of only two parameters. Therefore, if the Poisson's ratios of dissimilar materials are of interest, only one extra parameter needs to be included in the mechanical analysis accordingly.

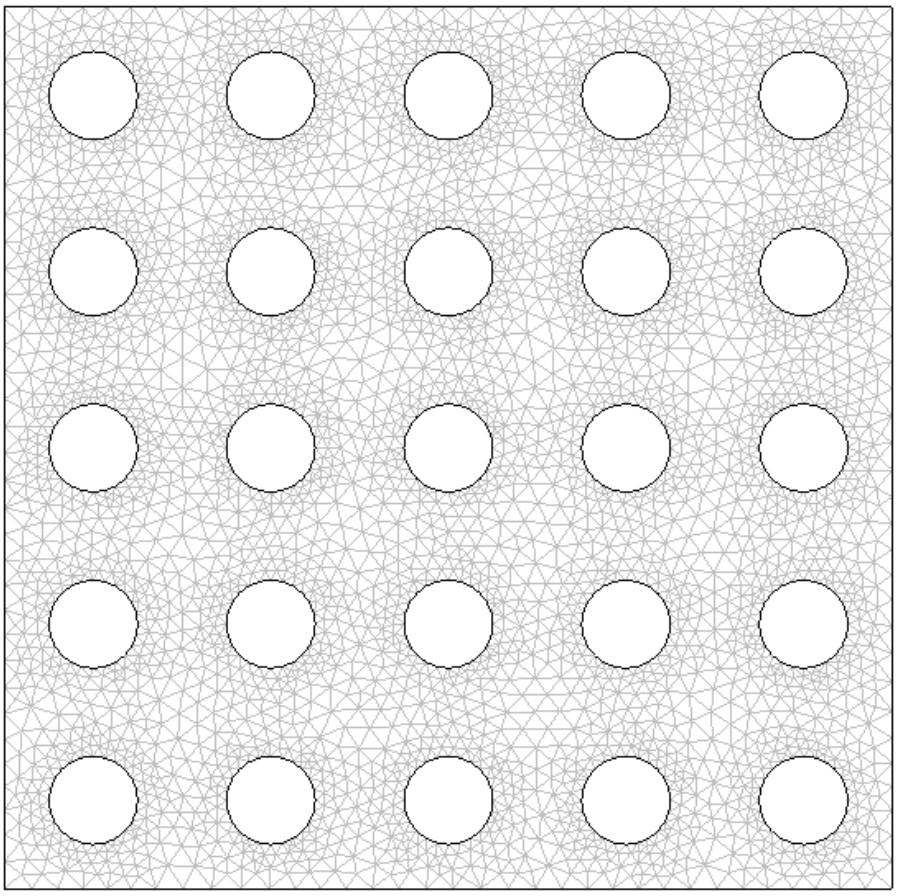

Figure 3-1 (a) Finite element model of a unit square plate containing uniformly distributed circular voids with 19.6% void volume fraction

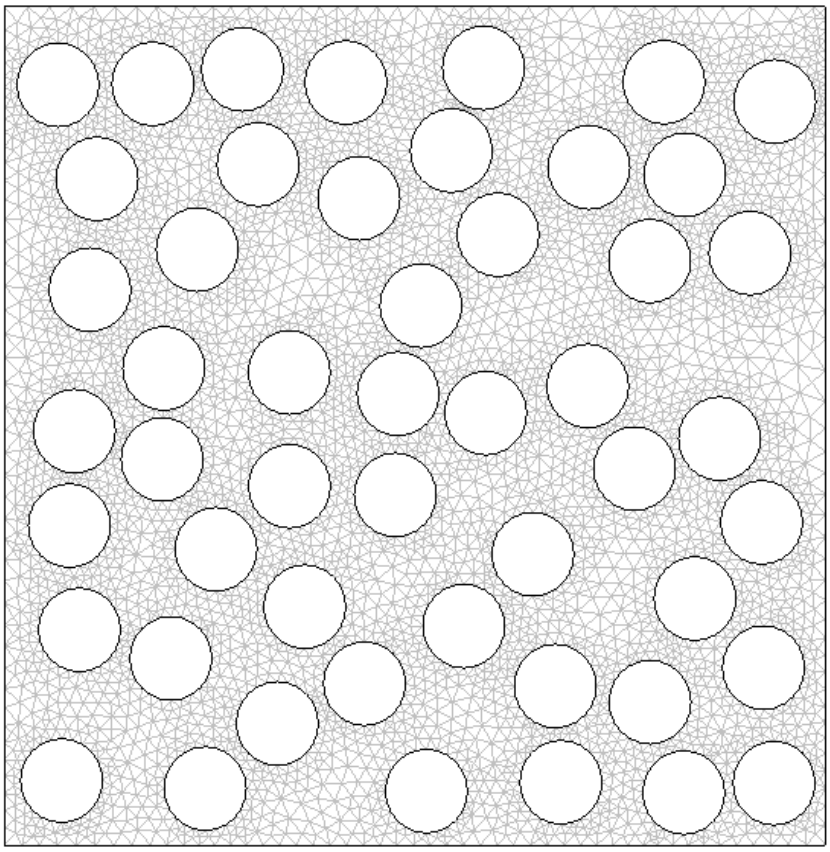

Figure 3-1 (b) Finite element model of a unit square plate containing randomly distributed circular voids with 38.5% void volume fraction.

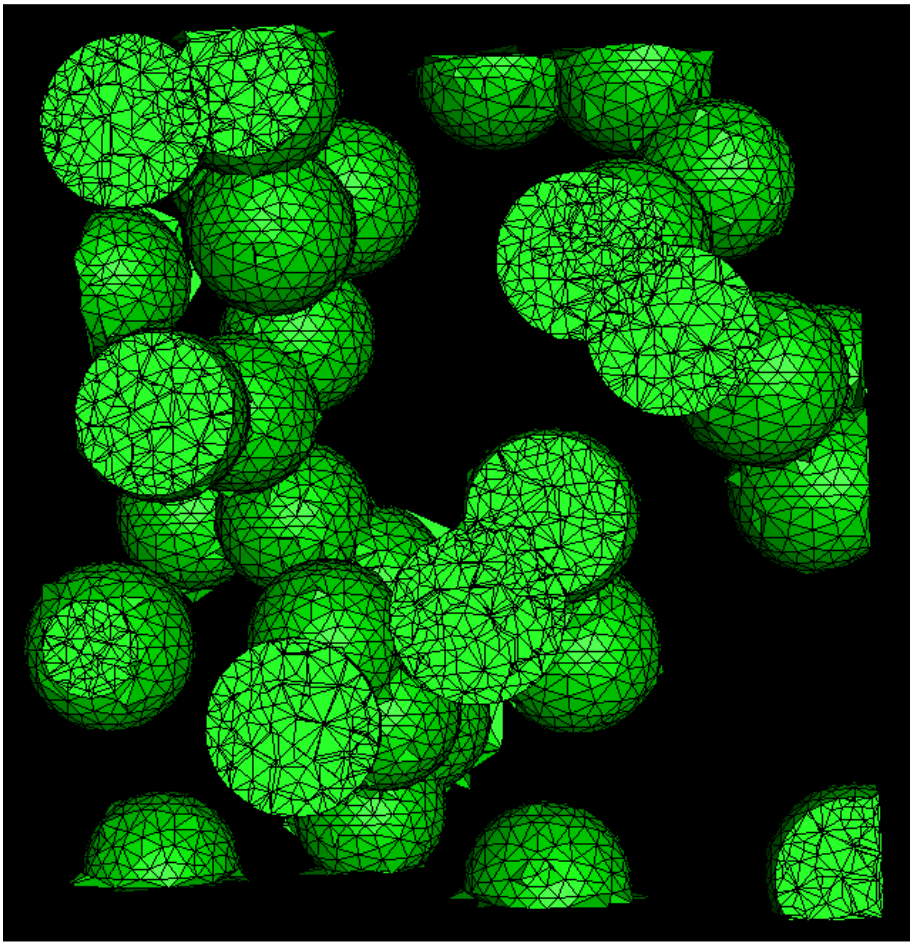

Figure 3-2 (a) 3-D finite element model in a unit cubical domain for overlapping spherical particles, and (b) cross section along the mid plane of the matrix with spheres removed.

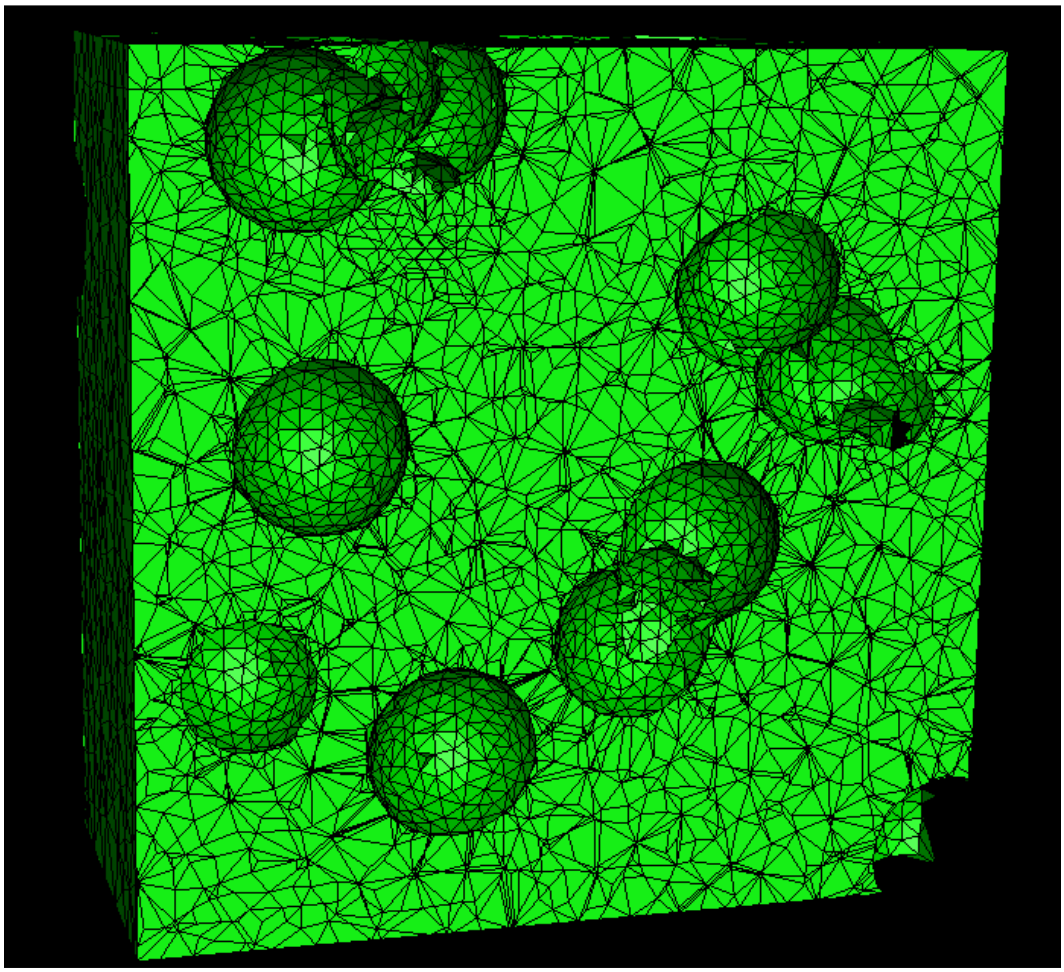

Figure 3-2 (b) 3-D finite element model in a unit cubical domain for a cross section along the mid plane of the matrix with spheres removed.

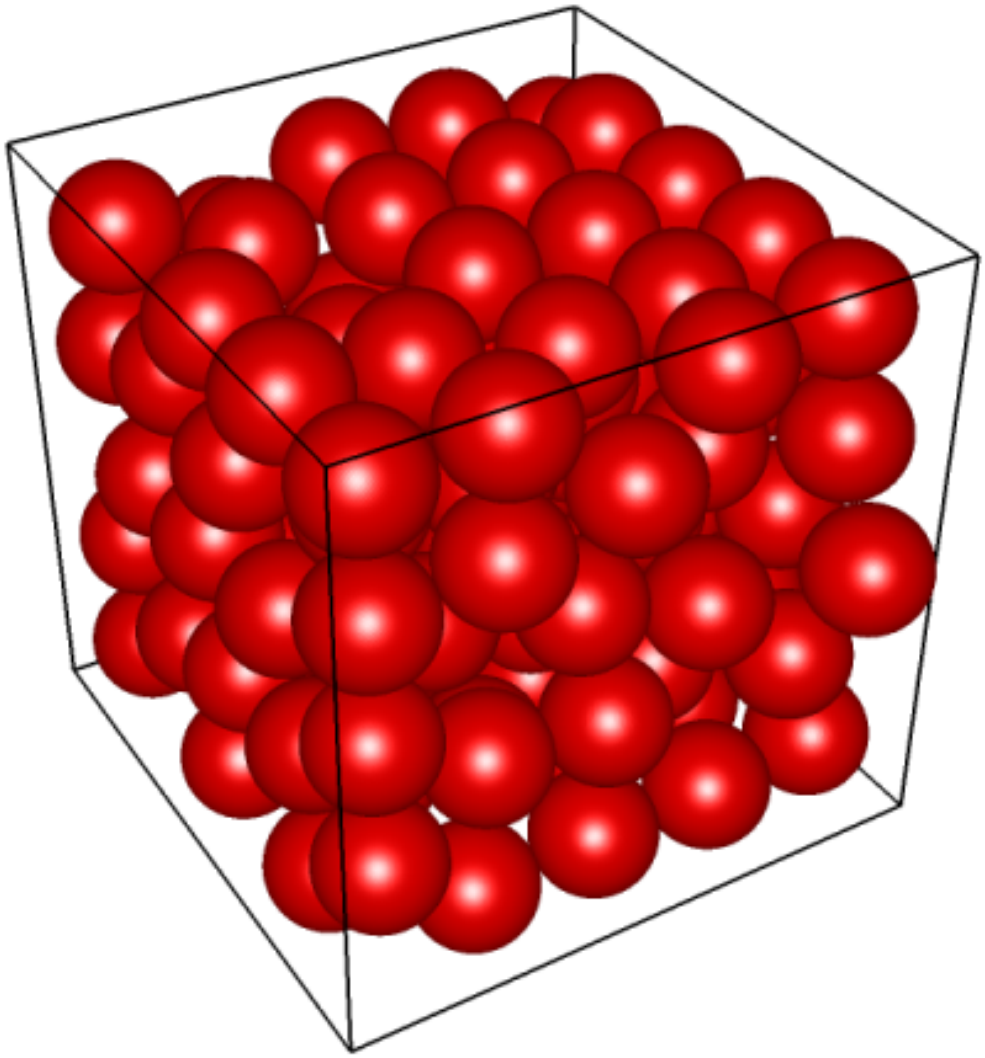

Figure 3-3 (a) Computer generated model of nonoverlapping spheres.

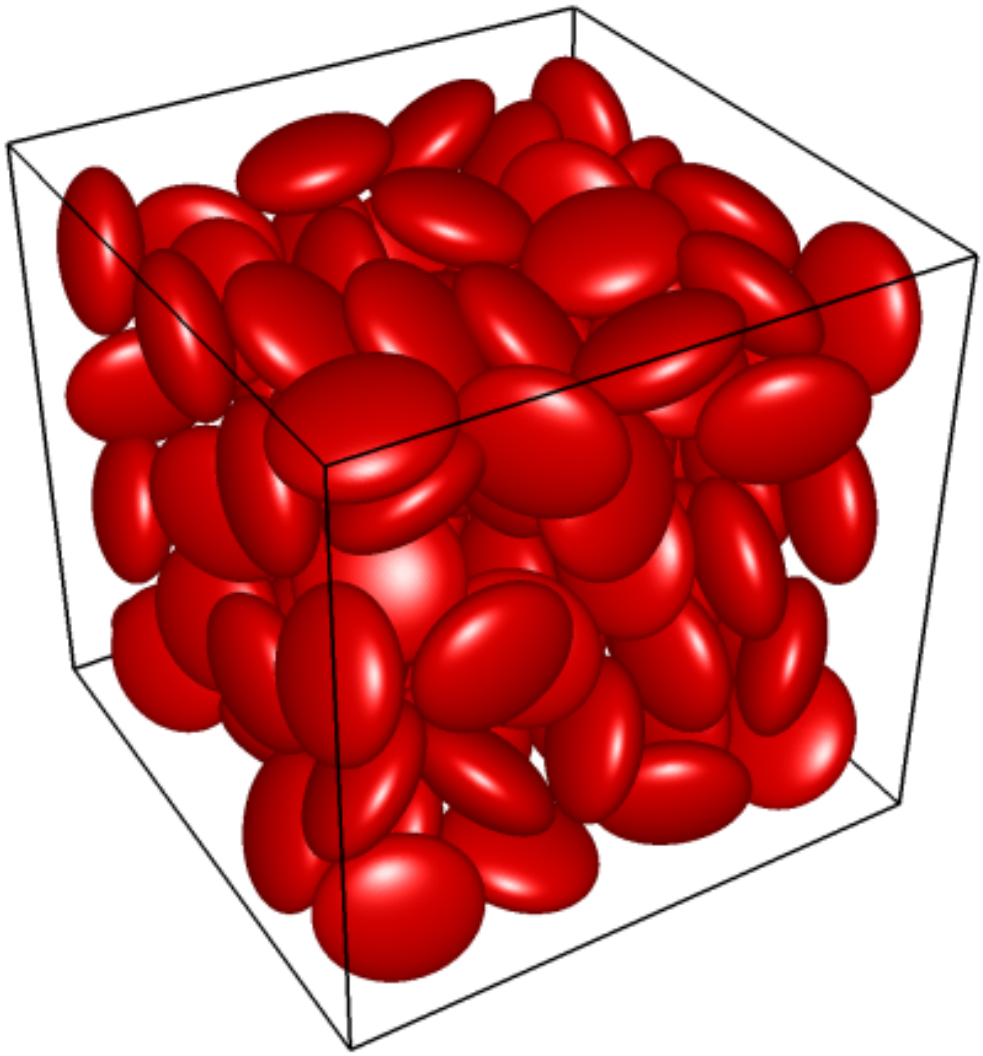

Figure 3-3 (b) Computer generated models of nonoverlapping ellipsoids.

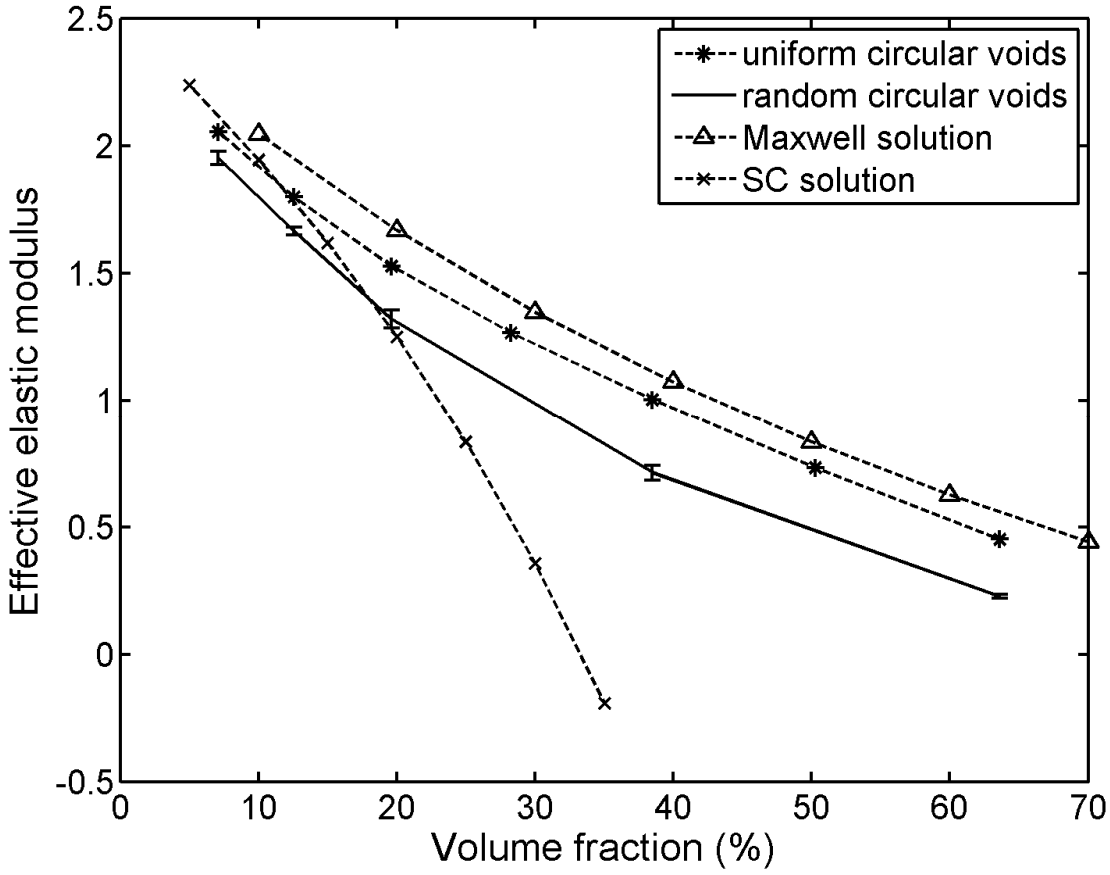

Figure 3-4 Comparison of normalized elastic modulus between simulations and effective medium approximations for both uniform and random circular void models.

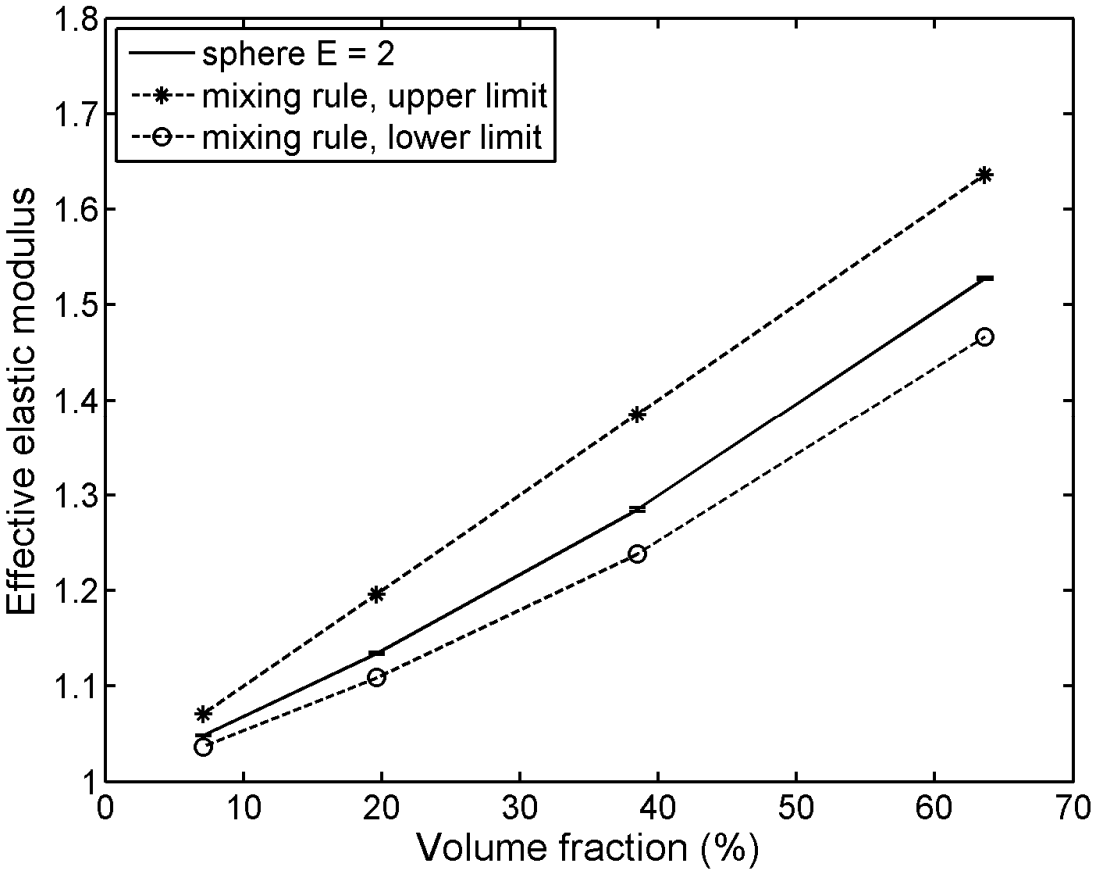

Figure 3-5 (a) Comparison of normalized elastic modulus between simulations and linear rules of mixing for models containing nonoverlapping random circular inclusions, with E_2 =2.

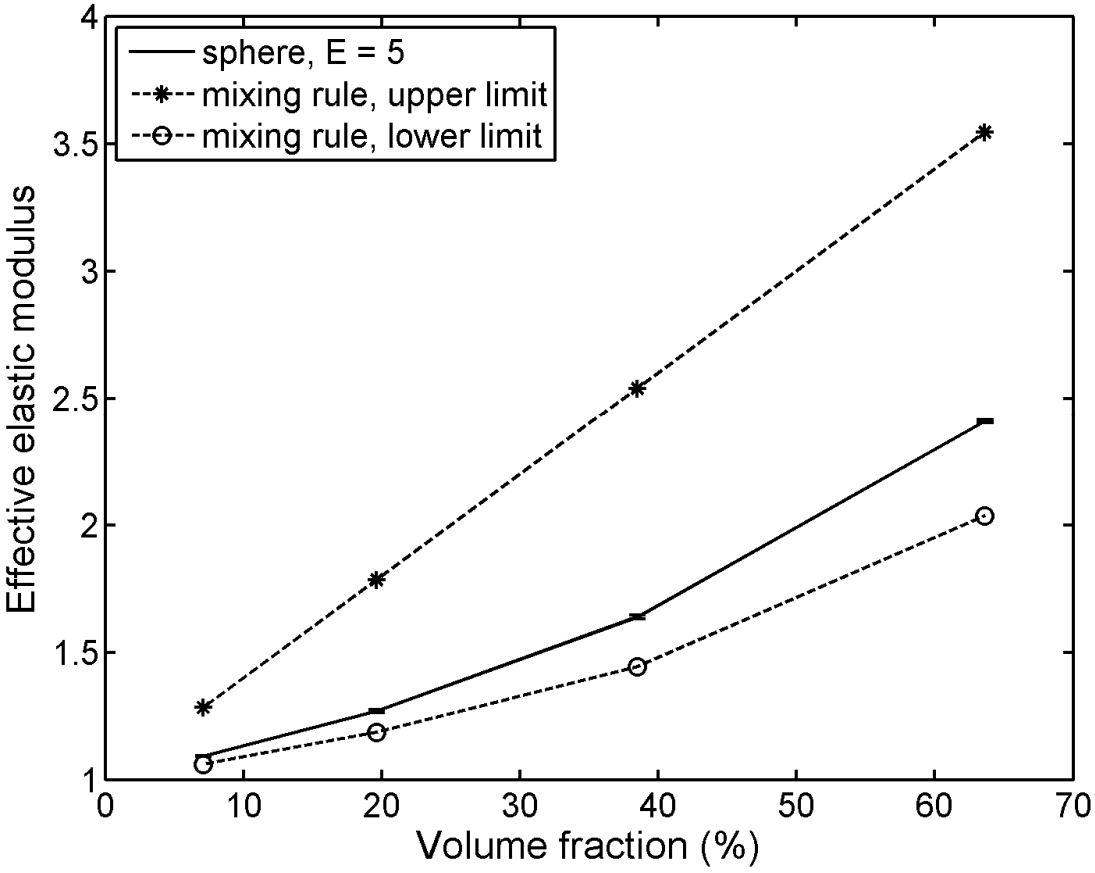

Figure 3-5 (b) Comparison of normalized elastic modulus between simulations and linear rules of mixing for models containing nonoverlapping random circular inclusions, with E_2=5.

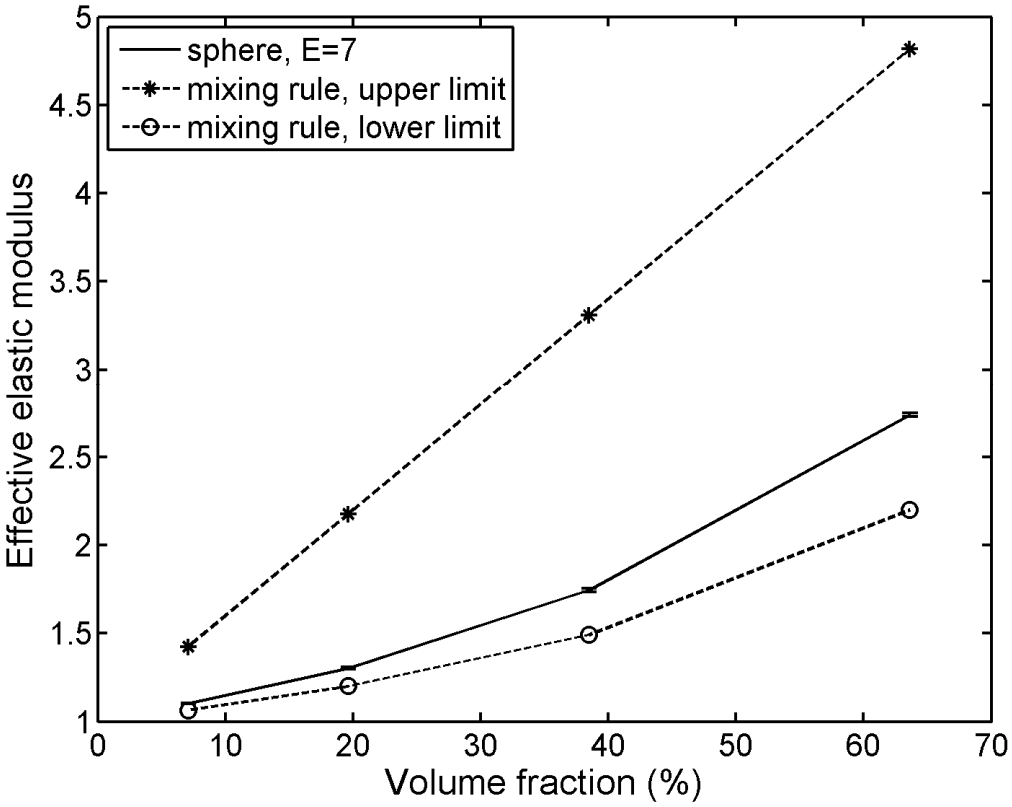

Figure 3-5 (c) Comparison of normalized elastic modulus between simulations and linear rules of mixing for models containing nonoverlapping random circular inclusions with E_2=7.

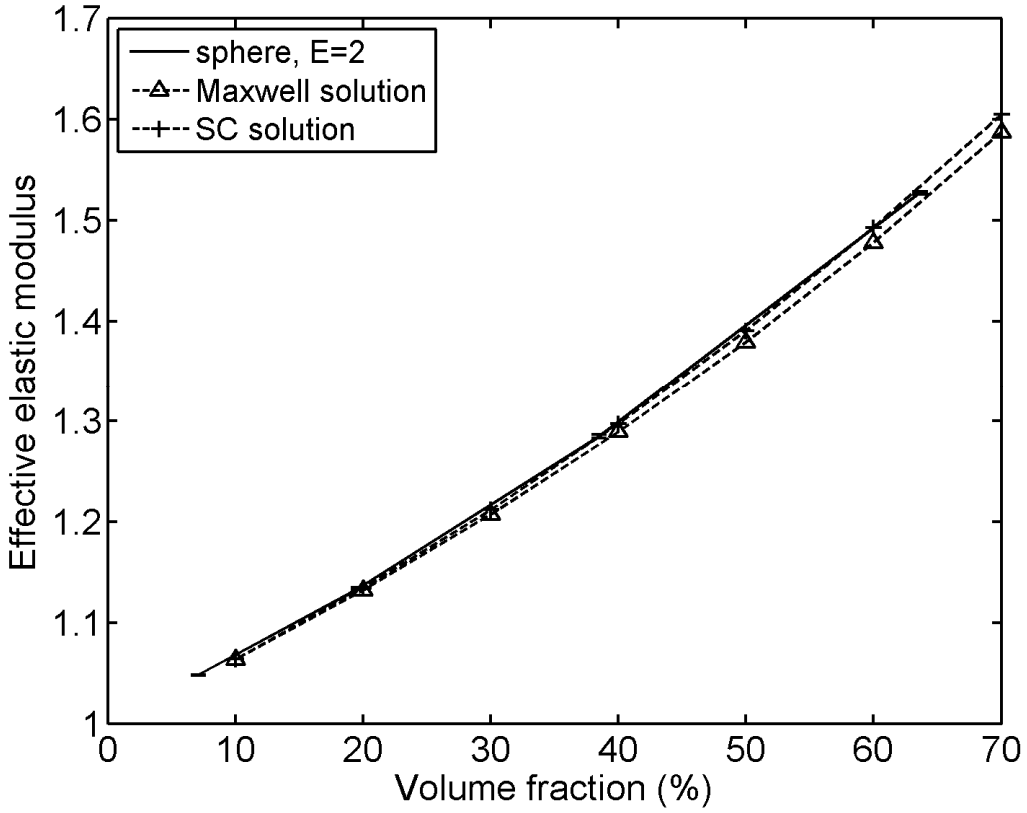

Figure 3-6 (a) Comparison of normalized elastic modulus between simulations and effective medium solutions for models containing nonoverlapping random circular inclusions with E_2=2.

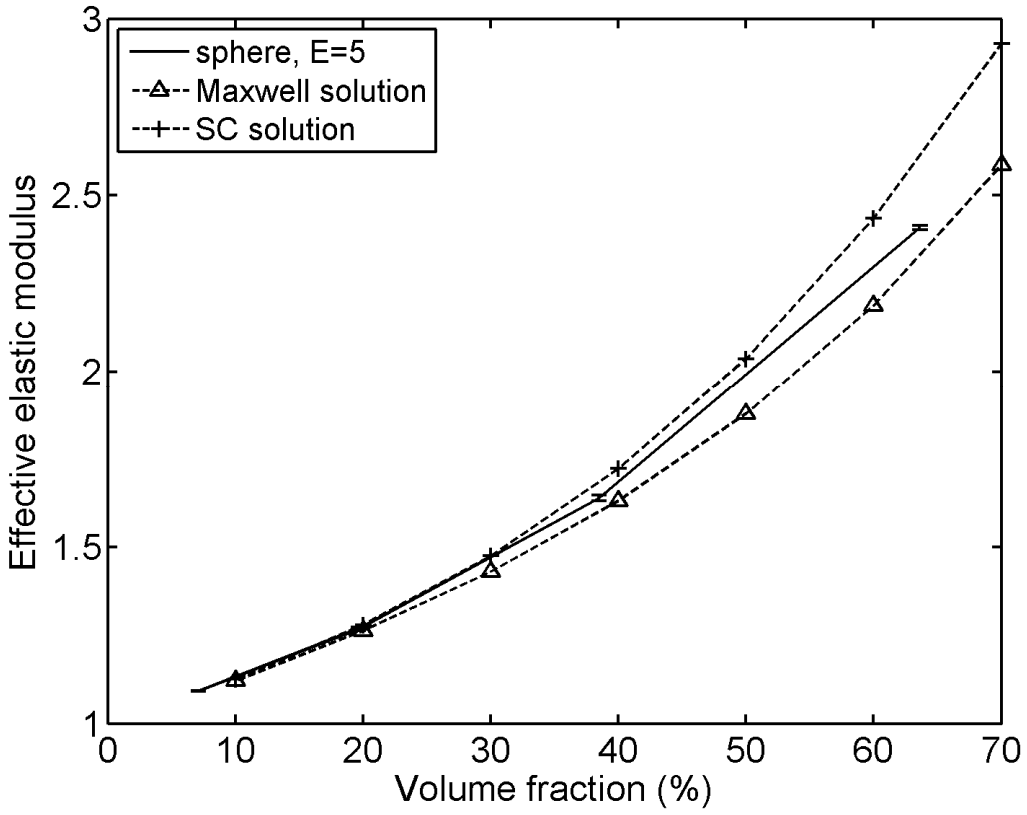

Figure 3-6 (b) Comparison of normalized elastic modulus between simulations and effective medium solutions for models containing nonoverlapping random circular inclusions with E_2=5.

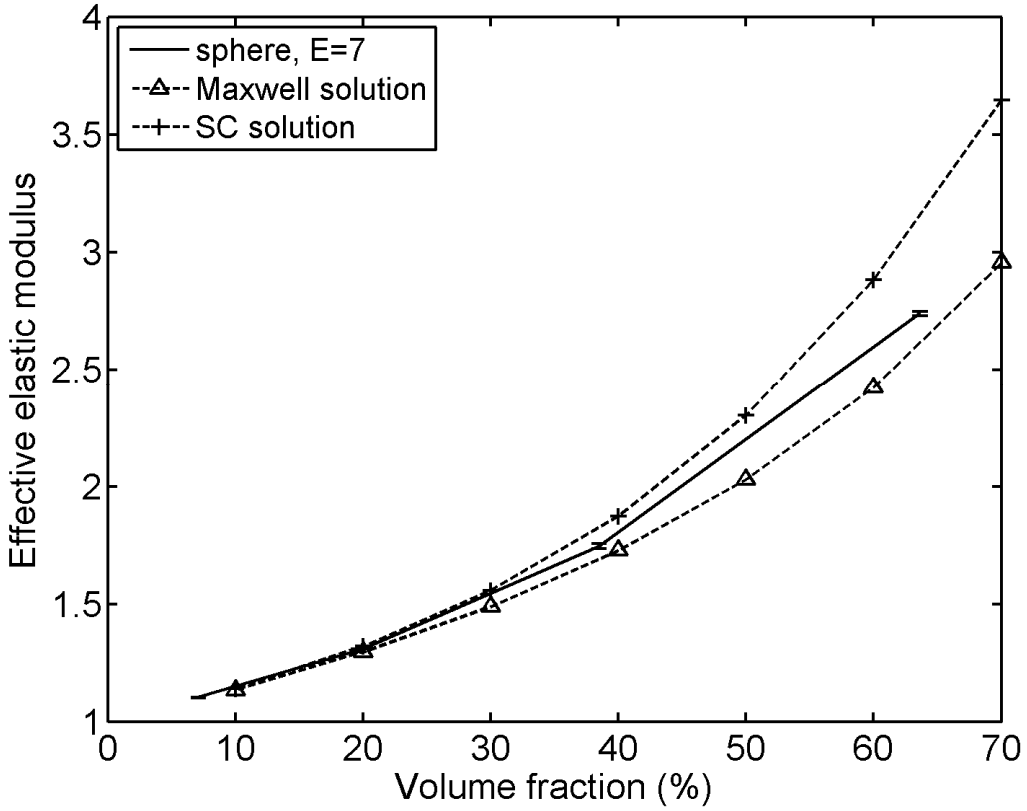

Figure 3-6 (c) Comparison of normalized elastic modulus between simulations and effective medium solutions for models containing nonoverlapping random circular inclusions with E_2=7.

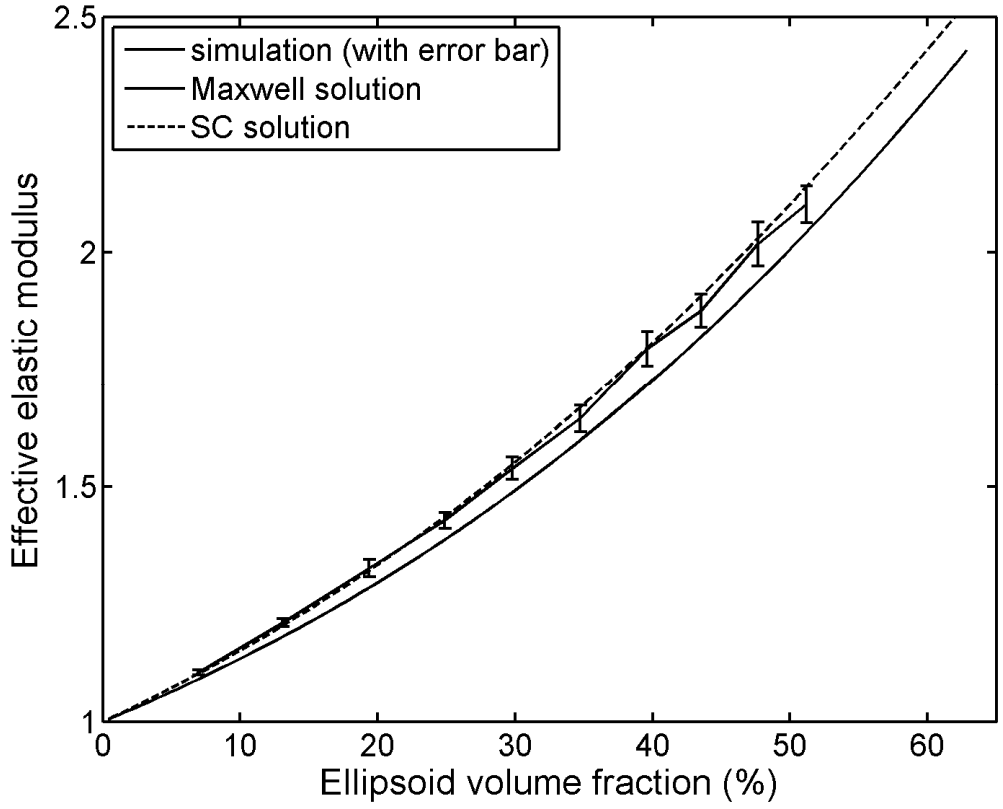

Figure 3-7 Comparison of normalized elastic modulus between simulations and effective medium solutions for models containing overlapping random spheres, with E_2=4.

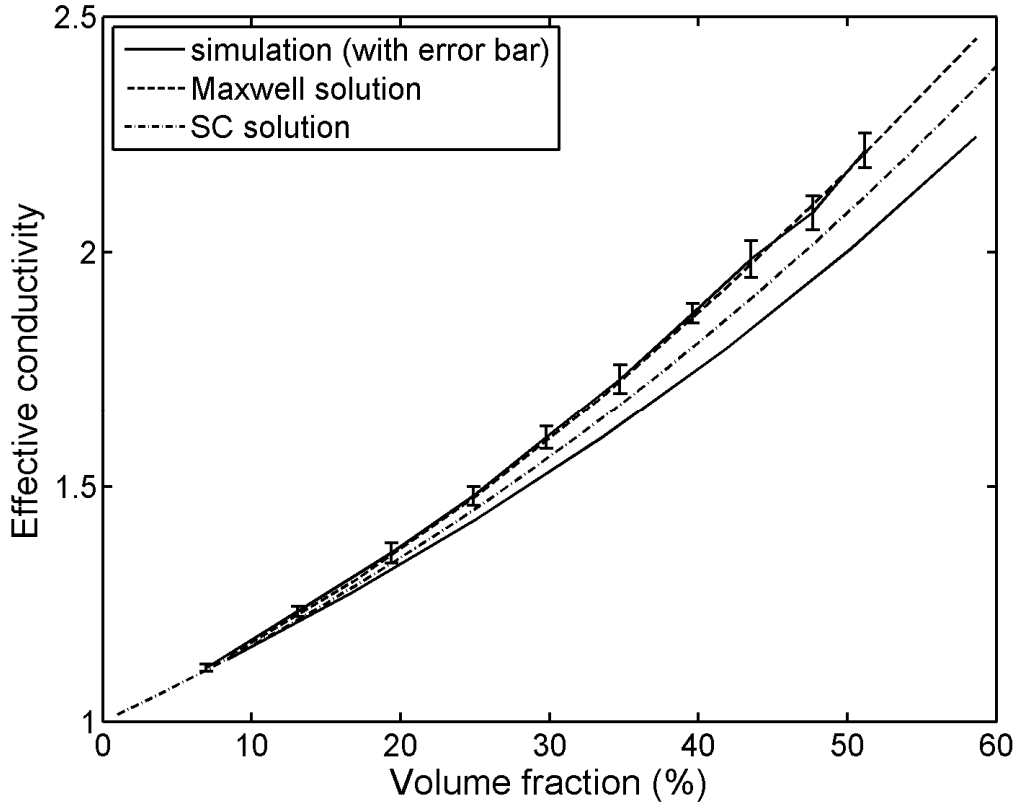

Figure 3-8: Comparison of normalized conductivity between simulations and effective medium solutions for models containing overlapping random spheres, with σ_2=4.

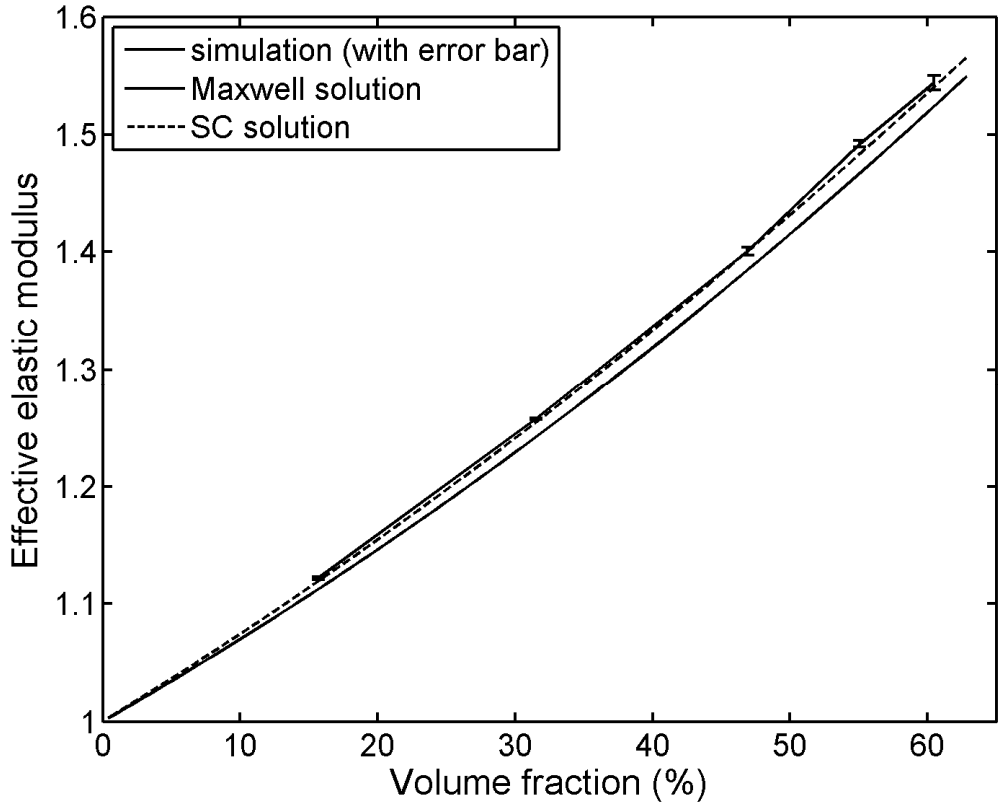

Figure 3-9 (a) Comparison of normalized elastic modulus between simulations and effective medium solutions for models containing nonoverlapping random spheres, with E_2=4.

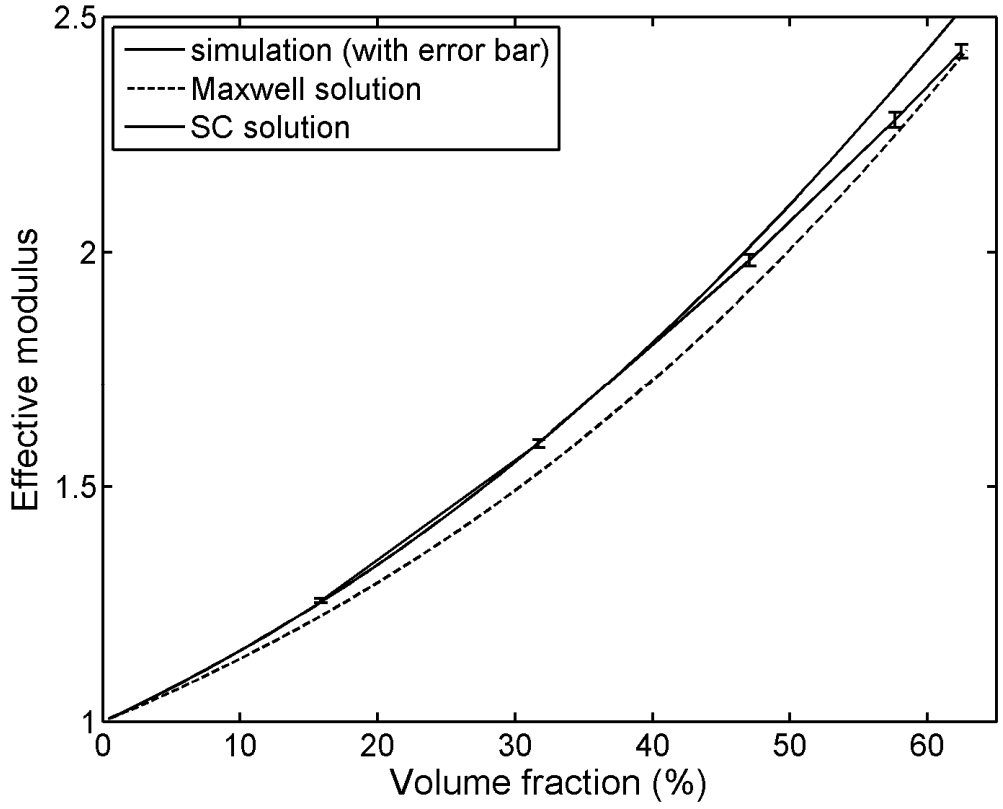

Figure 3-9 (b) Comparison of normalized elastic modulus between simulations and effective medium solutions for models containing nonoverlapping random spheres, with E_2=4.

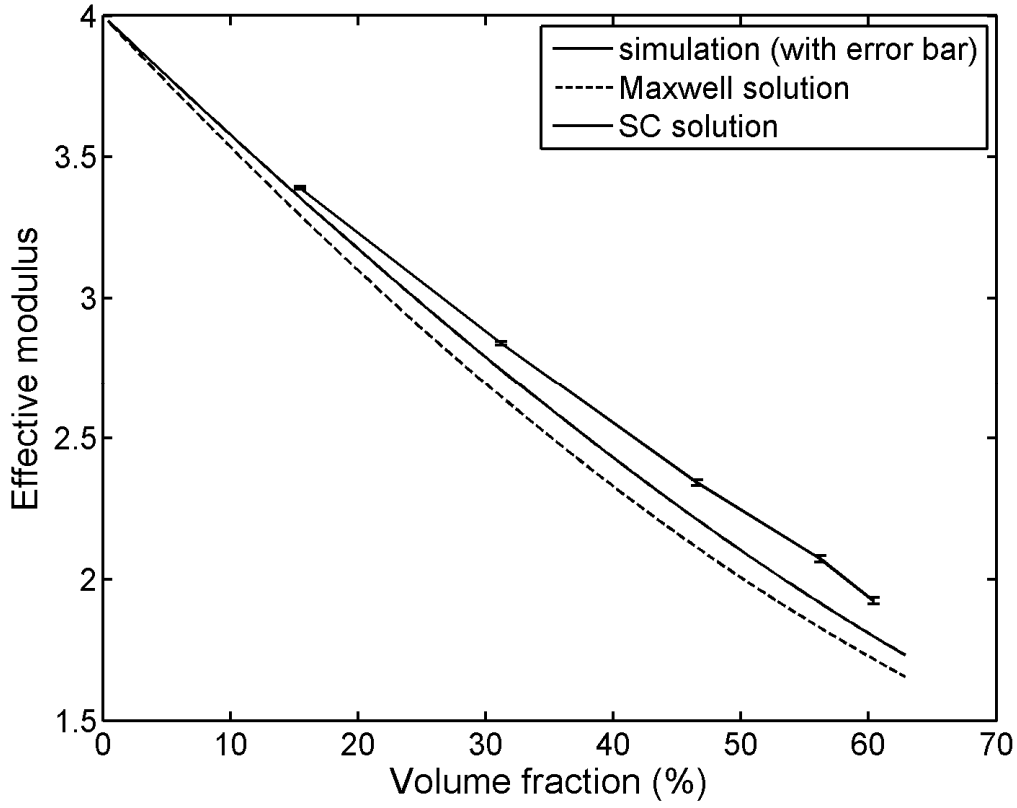

Figure 3-9 (c) Comparison of normalized elastic modulus between simulations and effective medium solutions for models containing nonoverlapping random spheres, with E_2=4.

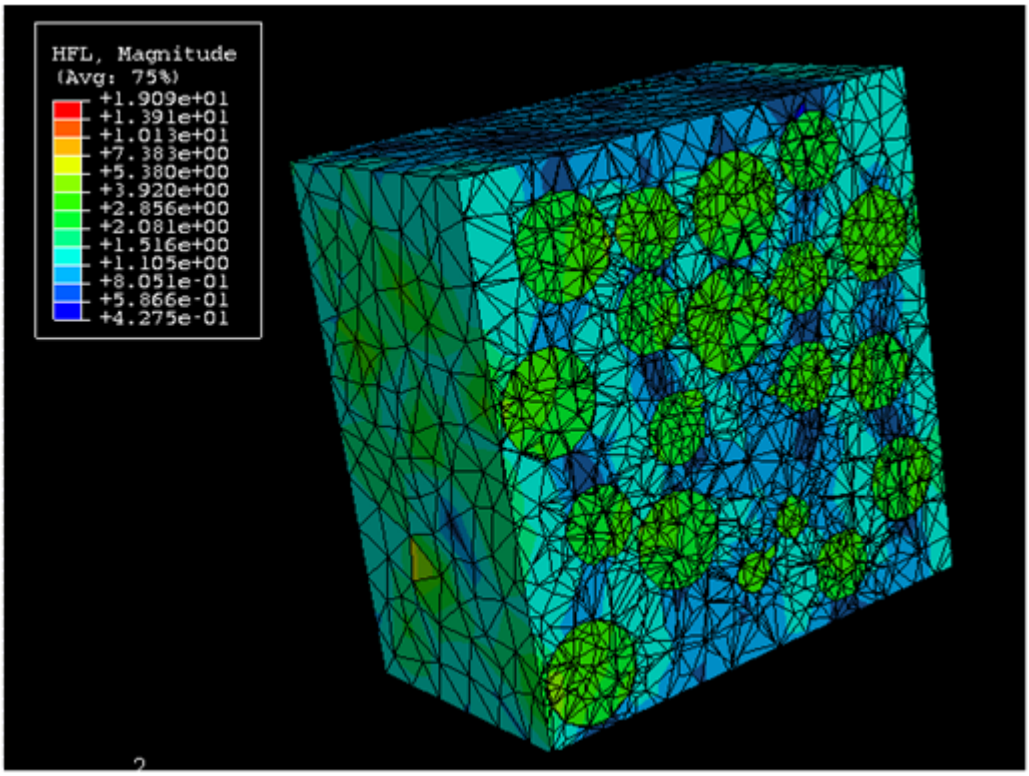

Figure 3-10 Von Mises stress distribution on the cross section along the mid-plane of the model studied in Fig. 9.

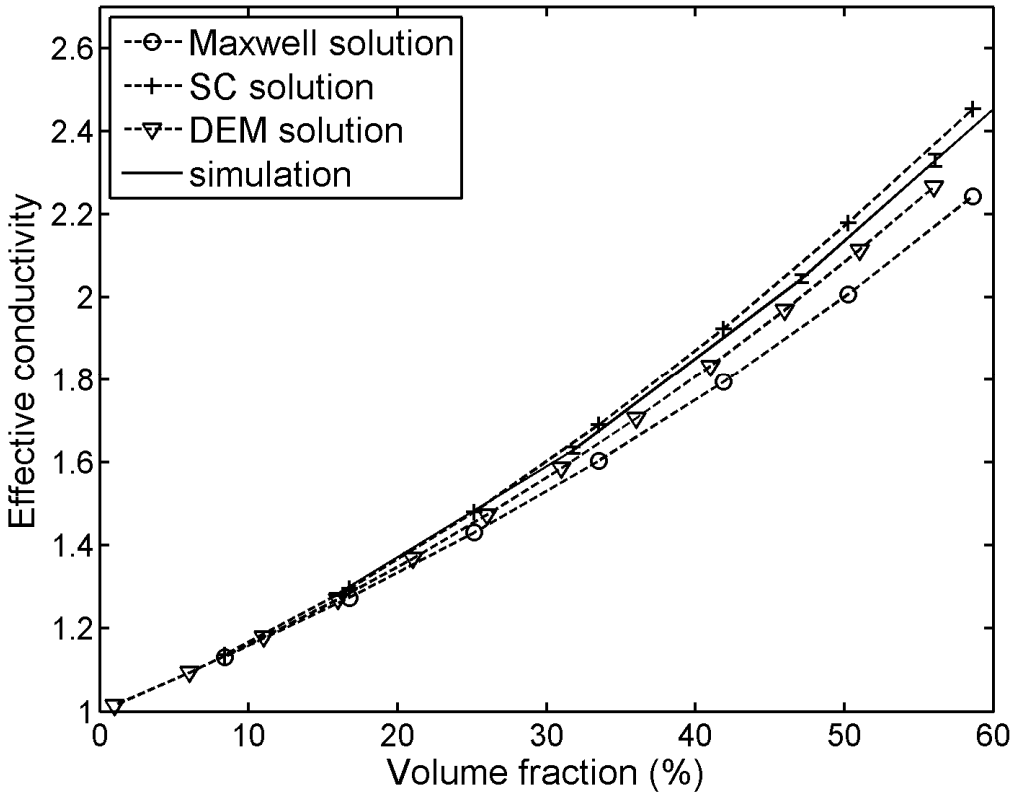

Figure 3-11 Comparison of normalized conductivity between simulations and effective medium solutions for models containing nonoverlapping random spheres, with σ_2=4.

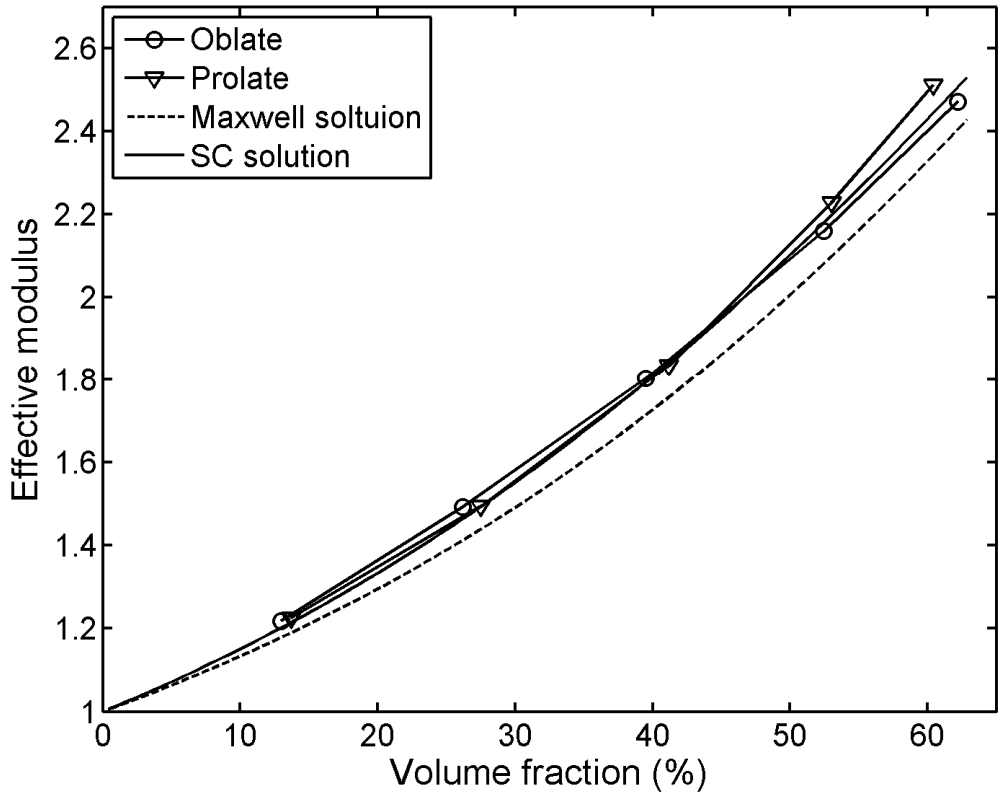

Figure 3-12 Comparison of normalized elastic modulus between simulations and effective medium solutions for models containing nonoverlapping random ellipsoids, with E_2=4 and ε=1.4.

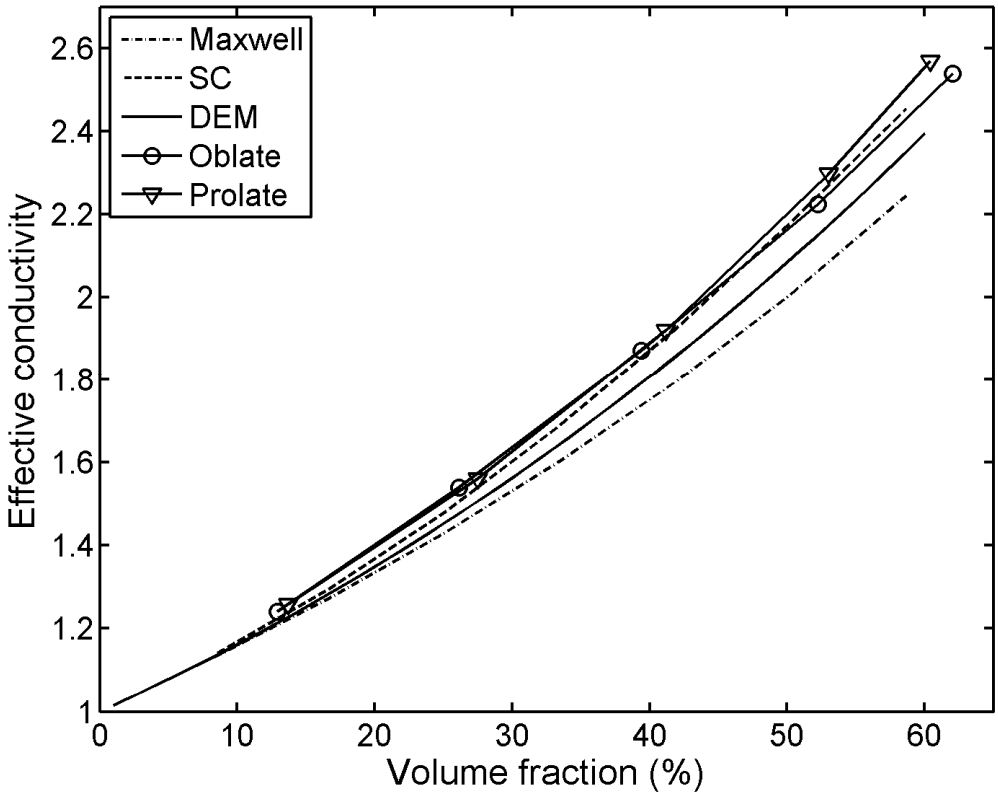

Figure 3-13 Comparison of normalized conductivity between simulations and effective medium solutions for models containing nonoverlapping random ellipsoids, with σ_2=4 and ε=1.4.

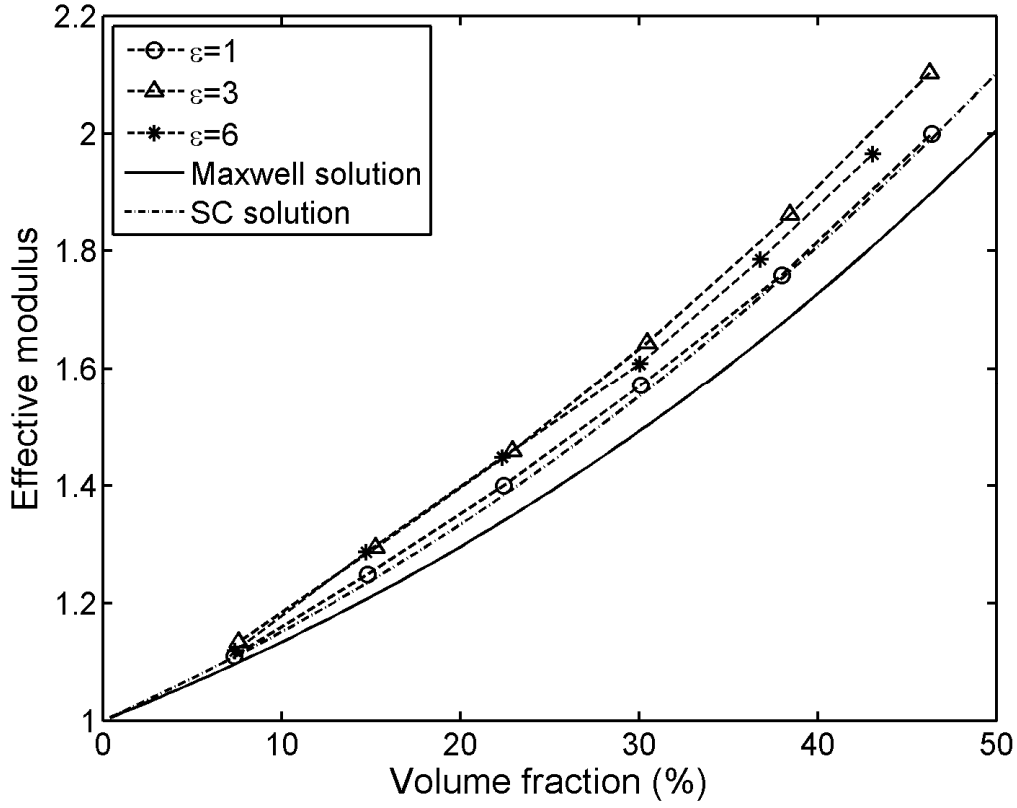

Figure 3-14 (a) Effect of ellipsoid aspect ratio on effective elastic modulus for equivalent spherical radius=0.1.

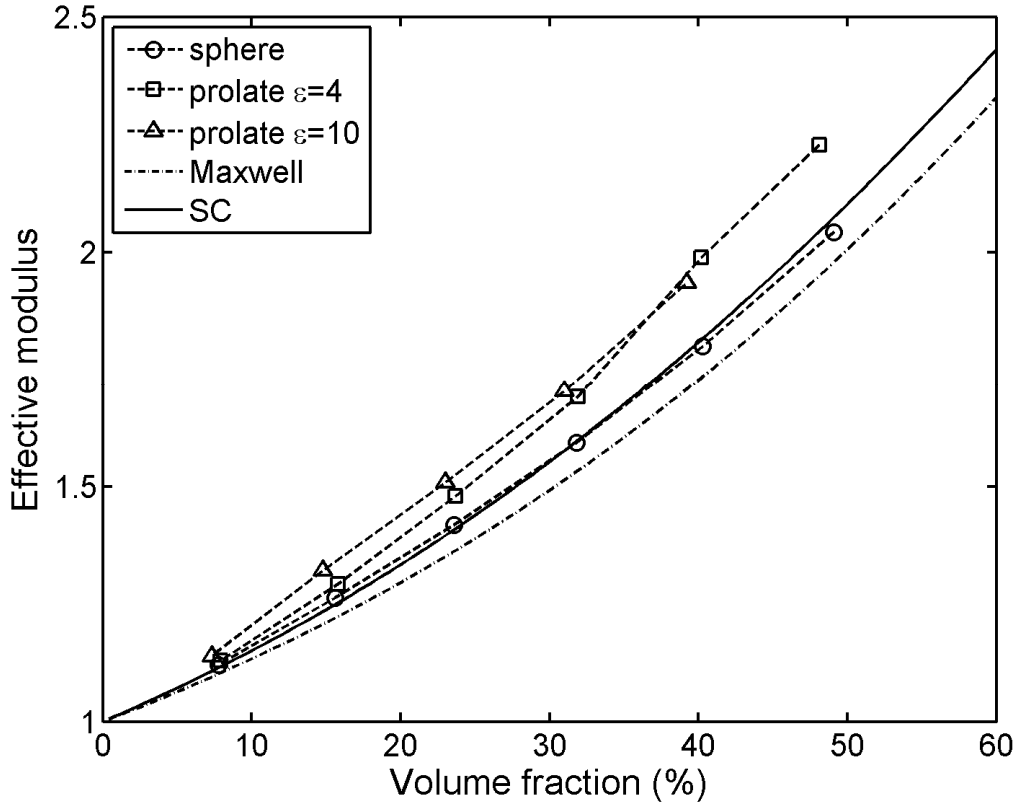

Figure 3-14 (b) Effect of ellipsoid aspect ratio on effective elastic modulus for equivalent spherical radius=0.05.

CHAPTER 4 GEOMETRIC PERCOLATION THRESHOLDS OF INTERPENETRATING PLATES IN THREE-DIMENSIONAL SPACE

4.1 Introduction and Literature review

Around 1940s, Floy and Stockmayer applied the concept of percolation theory to explain the formation of macromolecules from small branches of molecules. Broadbent and Hammersley (1957) introduced the percolation theory in more mathematical fashion namely in Hammersley publication “Percolation Structures and Processes” (Deutscher, 1983). The percolation theory and its emphasis on its critical phenomena was developed sine 1970s according to Essam and Gwilym (1971). Percolation or similar words appears almost in a hundred publications yearly, yet percolation theory is not easy to deal with even though its principle is quite simple.

Fundamentally, percolation phenomena can be introduced by the following simple explanation. Figure 4-1 shows a computer generated sample of 60×50 square lattice, array of squares, with probability $p \geq 0.6$ one cluster, group of neighbor dots, extends from one side to the other side. The point where the path from top to bottom or form left to right exist or formed, percolating cluster, called critical phenomena or percolation

threshold p_c (Stauffer, D. & Aharony, A., 2003). To illustrate this phenomenon from simulation point of view, one can show figure 4-2 in which percolation path or paths are generated spontaneously from the left side to the right side in a stochastic network system (Yi, & Sastry, 2002). These particles represent the conductive part in conductive media. Even though the inclusion part may vary, the concept of percolation is still the same.

In other words, percolation is referred to as a phenomenon where at least one domain spanning pathway exists in a physical system. It is closely related to the transport of mechanical properties of multiphase materials. Regardless of the interfacial contact among different material phases, measurement of the geometric percolation threshold, i.e. the minimum amount of materials required for percolation, is often one of the fundamental tasks in design and optimization of these materials (Mohanty, & Sharma, 1991,Yi, 2008). Mathematically, general percolation processes and phenomena have been studied in the past decades, via development of exact or approximate solutions in a finite or infinite field (Torquato, 2002). The fact that higher aspect ratio phases percolate at lower volume or area fractions in both two-dimensional (2-D) and three-dimensional (3-D) systems has been well documented, but the quantitative determination of the geometric effects on noncircular or nonspherical particles were relatively recent, due to the intensive computation demanded in the work.

Among the two primary means of estimating percolation points, namely the analytical approximation (Coniglio, Deangelis, Forlani, & Lauro, 1977; Quintanilla, & Torquato, 1996), and the Monte Carlo simulation (Pike, & Seager, 1974; Dhar, 1990), the latter has proved more computationally effective, especially for 3-D systems. Extensive

work on circular plates or spheres exists in the literature, including the measurement of the percolation threshold for fully penetrable disks of the same size using the frontier-walk method For example, in their study of the percolation threshold for fully penetrable discs, for efficiently, Quintanilla and Torquato (2000) applied the frontier method to calculate the percolation threshold, the gap-transversal method and the frontier-walk method. In the first one, an initial disc is located near the right-hand edge, and discs are generated gradually to the left until reaching the frontier in three steps Figure 4-3 exhibits the arcs generated in the boundaries of interior voids. In the second method, Frontier-walk method, a frontier of arbitrary length is created by cycling through the unit square. The advantage of this approach is that the generation of separate realizations process is no longer needed. It was found that the results, shown in figure 4-4 and table 4-1, are in agreement with previous estimates of the percolation threshold.

In addition, the determination of the critical threshold and exponents for hyperspheres was investigated, and it was found that the percolation threshold was considerably smaller than the reported values for smaller systems. This disagreement is related to the fact that the previous works' estimationa were too high (Rintoul, & Torquato, 1997). Percolation problems for disks or spheres of different radii were investigated by a binary mixture of particles (Quintanilla, 2001; Consiglio, Baker, Paul, & Stanley, 2003). One interesting finding of these works is that the percolation threshold of such a system is typically very close to that of equisized particles. For example, for a half-and-half mixture of smaller and larger particles, the difference in the percolation threshold is lower than 1% for both spheres and circular disks. Quintanilla and Ziff (2007) investigated asymmetry in the percolation thresholds of fully penetrable disks

with two different radii. It was shown that the percolation threshold as a function of volume fraction v and fixed ratio λ .is nearly symmetric and there is no theoretical expiations regards this issue. Figure 4-5 exhibits estimates of the percolation threshold for disks' aspect ratio range from 0.1 to 0.35, and by analyzing the symmetry in the graph, it was reported that the curves are slightly asymmetric.

Additionally, the research activities on percolation of disks and spheres were not only limited to solid material phases but also extended to void phases, namely "void percolation" (Yi, 2006). More complex geometries involving additional parameters have also been studied, including solid or hollow fibers and tubes (Berhan, Yi, Sastry, Munoz, Selvidge, & Baughman, 2004). It was reconfirmed that the percolation threshold is strongly dependent on the particle aspect ratio, implying that much fewer materials are needed for percolation of fibers or other high aspect ratio particles, thus merit the use of material inclusions of elongated shapes. For elliptical particles, simulation results were obtained from circles to needles, and an interpolation formula was developed that was believed superior to all other effective-medium theories (Xia, & Thorpe, 1988; Yi, & Stastry, 2002). For ellipsoids, interests were centered on ellipsoids of revolution in which two parameters are needed to define the geometric shape (Garboczi, Snyder, Douglas, & Thorpe, 1995). The extreme oblate limit of plate-like particles to the extreme prolate limit of needle-like particles was studied extensively and their asymptotic solutions were derived from curve fitting. The effect of dimensionality, i.e. the crossover from 2-D to 3-D ellipsoidal systems, was also investigated computationally (Yi, Wang, & Satry, 2004). Finally, the continuum percolation for interpenetrating squares and cubes were also

studied using the Monte Carlo method, and the corresponding percolation threshold accurate to three decimal places was reported (Baker, D., Paul, G., Sreenivasan, S., & Stanley, H., 2002).

Regardless of these important works in the area, results are missing for a special category of the particulate geometry, i.e. 2-D disks oriented in the 3-D space. It is of particular interest because circular disks are the limiting cases of oblate ellipsoids of revolution when their thickness approaches zero. Compared to their ellipsoid counterparts, disk-shaped particles can percolate at a much lower volume fraction and therefore have potential applications in engineering practice. In addition, elliptical disks in the 3-D orientation correspond to a limiting case where the generalized triaxial ellipsoids have a degenerate axis. Discussions on the percolation threshold of triaxial ellipsoids (as opposed to ellipsoids of revolution), particularly in their degenerate scenarios, have never been attempted in the literature. Moreover, realistic material inclusions can rarely have perfect circular, spherical or ellipsoidal shapes. Instead they may possess corner angles and facets. How these geometric factors alter the percolation properties remains unknown. It is our intention in the present work to fill in this gap. We target the geometric effects on the percolation thresholds of disk-like particles by introducing four fundamental shapes: circles, ellipses, triangles and squares (as shown in figure 4-6). We first establish the intersection criteria for such geometries and then apply the scaling theories and linear regressions to estimate the percolation thresholds. Comparisons will then be made to infer the effects of geometry on the results.

4.2. Methods and Simulation Procedures

4.2.1 Percolation Detection

A standard computational algorithm for percolation checking has been implemented. In particular, random disk-like particles were generated in a unit cell domain (figure 4-7). The interparticle connectivity as well as the particle-boundary connectivity was checked using the appropriate criteria. The system percolates if there is a connected cluster across the entire domain. The process is intrinsically probabilistic for a finite system and the probability of percolation was determined as simply the ratio of the percolation to the total number of simulations performed. The disk number corresponding to a percolation probability of 50% was recorded as the percolation threshold. This was achieved by a linear interpolation of the percolation probability against the disk number. Results for each condition reported in the current study were generated using at least 5 separate realizations. Since the probabilistic variation of the results depends on the disk size or the total disk number, an algorithm was developed to make the process more efficient. In particular, the number of realizations was variable depending on the disk size. For larger disks, this number was set to a few hundred, whereas for smaller disks, it was set to between five and ten. This treatment was able to greatly reduce the variation in the results thus increase the solution accuracy.

The percolation threshold can in, principle, be expressed in terms of either area fraction for 2-D particles or volume fraction for 3-D particles. In the current work where disks are oriented in 3-D, because of percolation threshold should be consistent with that

of the equivalent 3-D system instead of 2-D system.the percolation threshold definition should be consistent with that of the equivalent 3-D systems. We define the following variable to measure the percolation threshold:

$$\eta = \frac{4}{3} n \pi r^3 \tag{4-1}$$

where r is the radius and n is the total disk number. For triangles and squares, r is the equivalent radius of the circular disk having the same area. When r approaches to zero, n will become infinite for percolation, but the value of η will approach an invariant η_c, which is defined here as the "percolation threshold" of the system throughout this chapter.

4.2.2 Intersection Criteria

For circular disks, given two arbitrary disks with radii r_i, normal vectors n_i and center locations (x_i, y_i, z_i) where i=1, 2. Define $\vec{R}$ as the position vector from 1 to 2 and also define the following variables:

$$\cos\alpha = \vec{h}_1 \cdot \vec{h}_2; \tag{4-2}$$

$$\xi = \vec{R} \cdot \vec{h}_1 / \sin\alpha; \tag{4-3}$$

$$\vec{h}_c = \vec{h}_1 \times \vec{h}_2; \tag{4-4}$$

$$x_a = \frac{\vec{R} \cdot \vec{h}_c}{|\vec{h}_c|} + \sqrt{r_2^2 - \xi^2}\ ; \tag{4-5}$$

$$x_b = \frac{\vec{R} \cdot \vec{h}_c}{|\vec{h}_c|} - \sqrt{r_2^2 - \xi^2}\ ; \tag{4-6}$$

$$y = \frac{\vec{R} \cdot (\vec{h}_1 \times \vec{h}_c))}{|\vec{h}_1 \times \vec{h}_c|} - \xi(\vec{h}_1 \cdot \vec{h}_2)\ ; \tag{4-7}$$

$$x_p = \sqrt{r_1^2 - y^2}\ , \tag{4-8}$$

then in the following two cases, the two circular disks will intersect:

Case1: $r_2^2 - \xi^2 > 0$ and $\{ x_a^2 + y^2 \le r_1^2$ or $x_b^2 + y^2 \le r_1^2 \}$; (4-9)

Case 2: $r_2^2 - \xi^2 > 0$ and $|y| < r_1$ and $\{ (x_a - x_p)(x_b - x_p) < 0$ or $(x_a + x_p)(x_b + x_p) < 0 \}$. (4-10)

For elliptical disks, there is no closed-form criterion available for checking geometric intersection. The computational strategy here is to take one disk (plate α) as a reference disk and choose the frame of reference such that the major and minor axes of the disk are aligned with *x*- and *y*- axes of the global coordinate system. The circumference of the other disk (plate β) is then divided into a number of small segments in search of the intersection point between the boundary of plate β and the plane formed by plate α.

Case 1: assume there are no intersections points between the line segments and plate α, and then the two disks do not intersect.

Case 2: assume there are two points of intersection (x_a, y_a) and (x_b, y_b) and

$$y_0 = \frac{y_a x_b - y_b x_a}{x_b - x_a};$$

(4-11)

$$k = \frac{y_b - y_a}{x_b - x_a};$$

(4-12)

$$A = \frac{1}{a^2} + \frac{k^2}{b^2},\ B = \frac{2y_0 k}{b^2},\ C = \frac{y_0^2}{b^2} - 1;$$

(4-13)

$$\Delta = B^2 - 4AC;$$

(4-14)

$$x_p = \frac{-B + \sqrt{\Delta}}{2A},\ x_q = \frac{-B - \sqrt{\Delta}}{2A},$$

(4-15)

where a and b are the half lengths of the major and minor axes of Disk α, respectively. Then, in the following case, the two disks intersect:

$$\Delta>0 \text{ and } \{ (x_a - x_p)(x_b - x_p) < 0 \text{ or } (x_a - x_q)(x_b - x_q) < 0 \}.$$

(4-16)

In all other situations, the disks do not intersect.

The same strategy is applicable to square and triangular disks that is, we choose one plate as the reference disk and discretize its boundary into line segments to find the points of intersection between these segments and the plane formed by the other disk. It is

then followed by examining the relative positions of these intersection points with respect to the square or triangular surface. However, the total number of the required line segments is greatly reduced here: only four line segments are needed for a square and three segments for a triangle, as opposed to a least twenty or thirty such segments needed for an ellipse. Hence the computational efforts can be greatly reduced for squares and triangles compared to elliptical plates.

The above intersection criteria have been validated by graphically realizing the particles in the 3-D space followed by an inspection of their physical connectivity. A minimum of a hundred random realizations were examined before they were actually implemented for percolation checking.

For the binary dispersion of disks of different radii, we focus our interest in circular disks of two different radii r_1 and r_2 where $r_1<r_2$. Assume the two types of disks have the same number and therefore f=0.5 where f represents the fraction of smaller disks. Define r as the mean radius, i.e. r= (r_1+r_2)/2, and $\lambda=r_1/r_2$, $0\le\lambda\le1$, then

$$r_1 = \frac{2\lambda r}{1+\lambda},\ r_2 = \frac{2r}{1+\lambda}. \tag{4-17}$$

Further, we fix the total disk number in this binary system while choosing the value r such that the corresponding η defined in Eq. (4-1) is maintained the same as that of the equisized disk system. If the equisized disks have radius r_0, then the relationship between r and r_0 is

$$r = \frac{(1+\lambda)r_0}{\sqrt[3]{4(1+\lambda^3)}} \tag{4-18}$$

Based on these assumptions, simulations can be performed in a procedure similar to equisized disk systems and the resulting percolation thresholds η_c can be evaluated.

4.3 Error Analysis

The numerical error associated with the extrapolated critical percolation point η_c can be estimated in the following method: assume there is a data array containing *n* pairs of *r* and η (r_i, η_i), according to the linear regression theory, we have

$$\eta = a_0 + a_1 r\,, \tag{4-19}$$

Where

$$a_1 = \frac{n\sum_{i=1}^{n}(r_i\eta_i) - \sum_{i=1}^{n} r_i \sum_{i=1}^{n} \eta_i}{n\sum_{i=1}^{n} r_i^2 - \left(\sum_{i=1}^{n} r_i\right)^2} \tag{4-20}$$

and,

$$a_0 = \frac{\sum_{i=1}^{n}\eta_i \sum_{i=1}^{n} r_i^2 - \sum_{i=1}^{n} r_i \sum_{i=1}^{n} r_i\eta_i}{n\sum_{i=1}^{n} r_i^2 - \left(\sum_{i=1}^{n} r_i\right)^2}$$

(4-21)

The corresponding confidence intervals for σ_{a0} and σ_{a1} are

$$\sigma_{a0} = \sigma_0 \sqrt{\frac{\sum_{i=1}^{n} r_i^2}{n\sum_{i=1}^{n} r_i^2 - \left(\sum_{i=1}^{n} r_i\right)^2}} \tag{4-22}$$

and

$$\sigma_{a1} = \sigma_0 \sqrt{\frac{n}{n\sum_{i=1}^{n} r_i^2 - \left(\sum_{i=1}^{n} r_i\right)^2}}, \tag{4-23}$$

where we assume that all the data points have the same confidence interval, σ_0 and

$$\sigma_0 = \sqrt{\frac{1}{n}\sum_{i=1}^{n}[y_i - (a_0 + a_1 x_i)]^2}\ . \tag{4-24}$$

Clearly, the critical percolation point η_c at r=0 is equal to a_0 and the associated standard deviation is equivalent to σ_{a0}.

4.3. Results and Discussion

The percolation algorithm was first validated against the equisized spheres system whose solution is well known. The simulation results are presented in figure 4-8. The percolation threshold was computed from nine different radii ranging from 0.007 to 0.04.

The total number of particles was from approximately 240,000 to 1,300, accordingly. To minimize the numerical error, the simulations were repeated 50 to 1,000 times for each particle radius and the computational time was approximately 70~150 Pentume (D) CPU hours for each radius. A linear regression was performed to estimate the percolation threshold corresponding to spheres of zero radiuses. The extrapolated solution η_c=0.3412±0.0003. This result corresponds to a volume fraction of 28.91%, which is fairly close to the currently most accurate solution 28.9573% obtained by Lorenz and Ziff (2001). This preliminary work can therefore be considered as a validation process for the percolation algorithm developed in the present study.

The same algorithm was subsequently applied to permeable circular plates in the 3-D space, and the results are shown in figure 4-9. These results were computed from 8 different radii ranging from 0.01 to 0.04, with the total number of particles ranging between 230,000 and 3,800, accordingly. The extrapolated solution is η_c=0.9614±0.0005. It should be pointed out that this result is noticeably lower than that reported by Garboczi, et al (Berhan, L., Yi, Y. B., Sastry, A. M., Munoz, E., Selvidge, M., & Baughman, R., 2004) They studied the oblate and prolate ellipsoids and provided an asymptotic solution for oblate particles of zero aspect ratio (that is, zero dimension through the thickness), which should be identical to the solution for circular disks. However, their prediction was 1.27 a/b in terms of the volume fraction of particles where b is the radius of revolution and a is the semi-axis length. Applying

$$f = 1 - \exp(-nV) \approx nV = \frac{4}{3} n\pi ab^2 \text{, when } a \to 0 \text{,} \tag{4-25}$$

where *f* represents the volume fraction, *V* is the volume of each individual particle, and *n* is the particle number, we have the formula

$$\eta_c = \frac{4}{3} n \pi b^3 \to 1.27, \tag{4-26}$$

which is obviously much higher than the result predicted in the current study (0.9614). The reason behind this discrepancy is yet unknown. It was noticed in the past that Garboczi's solutions for the percolation thresholds of overlapping ellipsoids were consistently higher than those predicted by other methods (Yi, & Sastry, 2004), and therefore it is not surprising to see the discrepancy in the comparison here.

For square-shaped disks in the 3-D space, the results are shown in figure 4-10. The maximum number of disks involved is 150,000. The extrapolated percolation threshold at zero size of squares is η=0.8647±0.0006. Clearly, this value is lower than that for circular plates, indicating that fewer particles are needed for percolation. This is because the corner angles of squares make it easier for the disks to touch each other, therefore reducing the percolation point. This is consistent with the corner effects elucidated in Baker et al.'s work regarding the continuum percolation of 2-D squares and 3-D cubes (Baker, Paul, Streenivasan, & Stanley, 2002).

The results for equilateral triangles are shown in figure 4-11. The maximum number of disks is around 430,000, and the predicted percolation threshold is η=0.7295±0.0006. Compared to the square-shaped disks, the triangles have slightly more elongated shape at the corners (60° angles in triangles as opposed to 90° angles in

squares), therefore facilitating the interparticle connectivity. As a result, the percolation threshold is further reduced. The above results, including the mean values and standard deviations for various geometries, are tabulated in Table 4-2.

The investigation on elliptical disks revealed that the percolation threshold monotonically decreases with the disk aspect ratio figure 4-12. At $\varepsilon=5$, η_c is only half the value at $\varepsilon=1$, meaning that much fewer particles are needed to reach percolation at higher aspect ratios. This is consistent with both the analytical and computational results reported in the literature. In addition, the results show that the reduction in the percolation threshold is not significant when the aspect ratio is below 1.5 but experiences a relatively sharp decrease beyond that point. This agrees with the predicted trends from other elongated particles such as ellipsoids reported in the literature (Garboczi, & Berryman, 2001). A maximum of 30,000 particles were realized in the simulations. Each aspect ratio was run for three different radii 0.02, 0.03 and 0.04 for linear extrapolation. Particles with aspect ratio greater than 5 were not studied due to the extremely intensive computation. However, it is expected that the percolation threshold will follow the same monotonic relationship with the aspect ratio beyond that point.

For the binary dispersion of circular disks, *f* was maintained to be 0.5 and λ was varied from 0.1 to 0.9 with an increment of 0.1 in the simulations. Notice that both $\lambda=0$ and $\lambda=1$ correspond to disks of the same size. Four different mean radii were examined to extrapolate the percolation threshold for each value of λ. The estimated percolation thresholds along were errors are listed in Table 4-3. Clearly, η_c increases at the beginning, reaches a peak value $\eta_c \approx 0.9815$ around $\lambda=0.5$, and then decreases. At the two

ends where λ is close to 0 or 1, η_c is approaching 0.9616. It is seen that for the entire range of λ, the deviation of η_c from the equisized disk solution is noticeably small- not more than 2%. A close inspection also shows the existence of the asymmetry in the result with respect to the midpoint λ=0.5. These results are consistent with Quintanilla's work on the binary dispersion of disks on a 2-D plane (Quintanilla, & Ziff, 2007) although a different peak value location (λ=0.4 when f=0.5) was reported for 2-D disks.

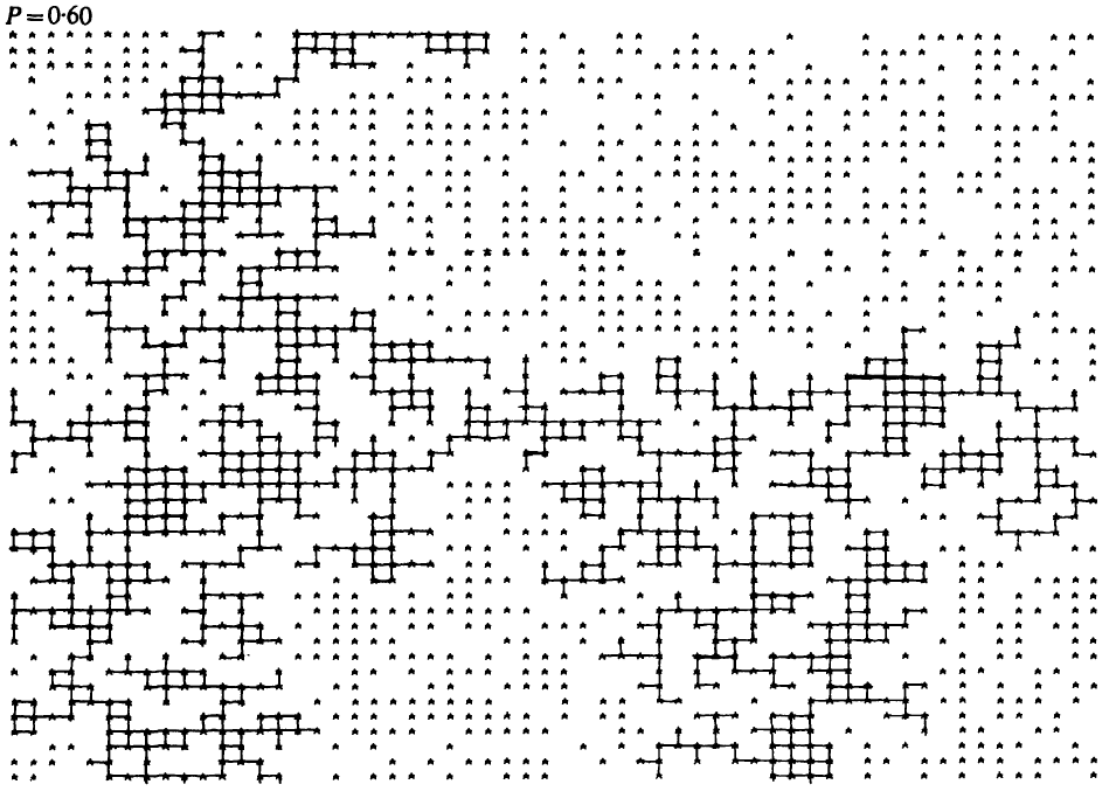

Figure 4-1 Example for percolation on a 60×50 square lattice, occupied squares are shown as *, empty squares are ignored.

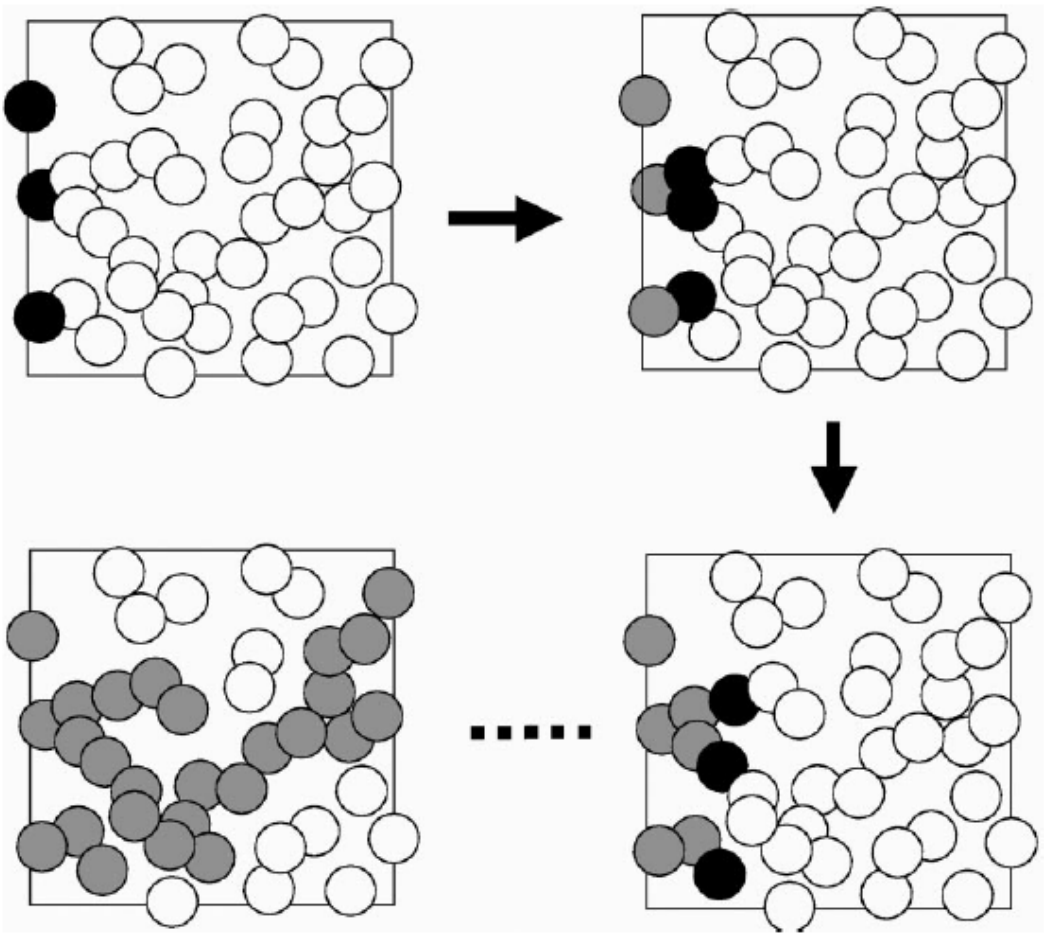

Figure 4-2 A Schematic depiction of the simulation algorithm for identifying percolation in a stochastic network system.

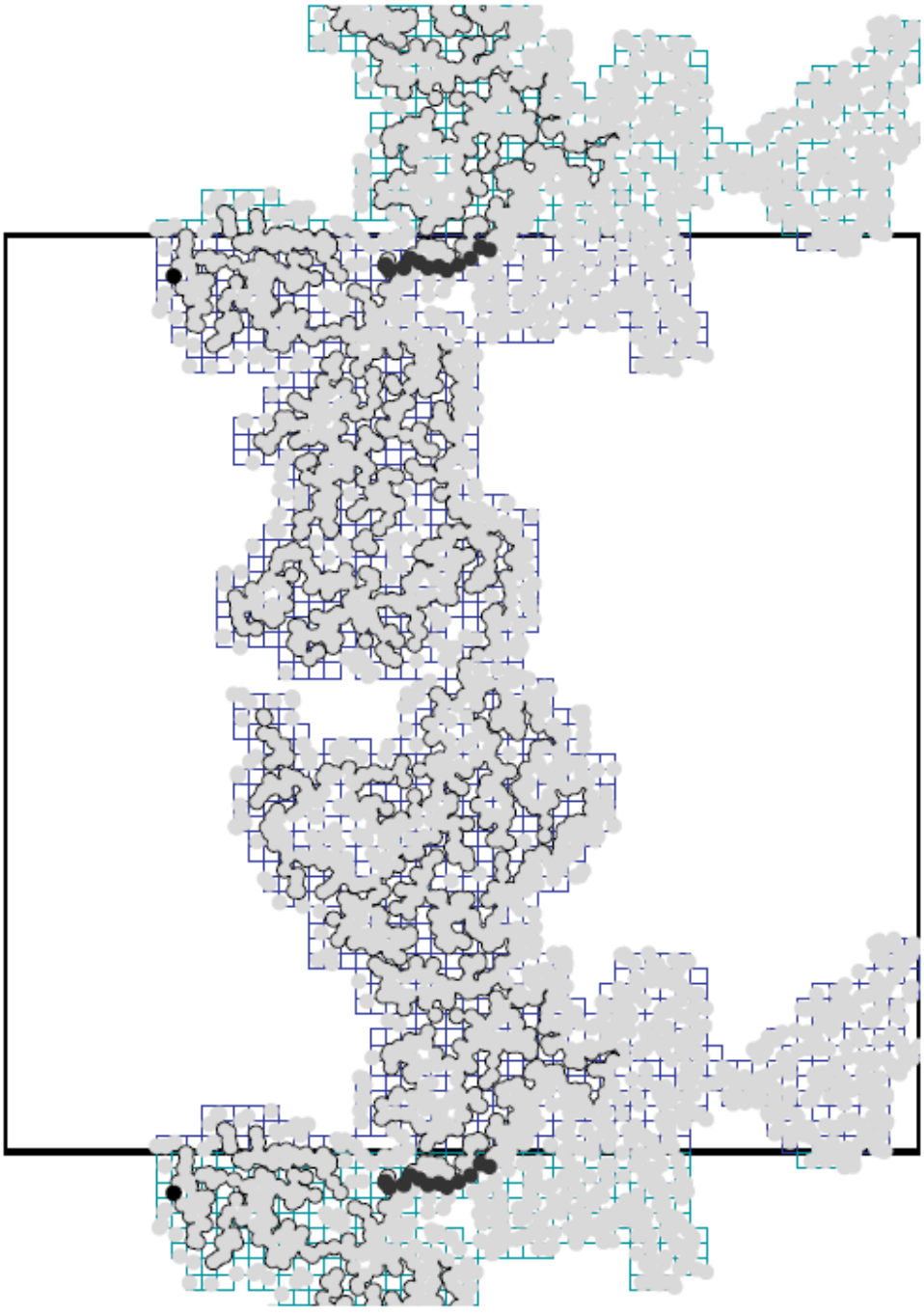

Figure 4-3 A simulated frontier for l=400 with a 60×60 grid of subsquares.

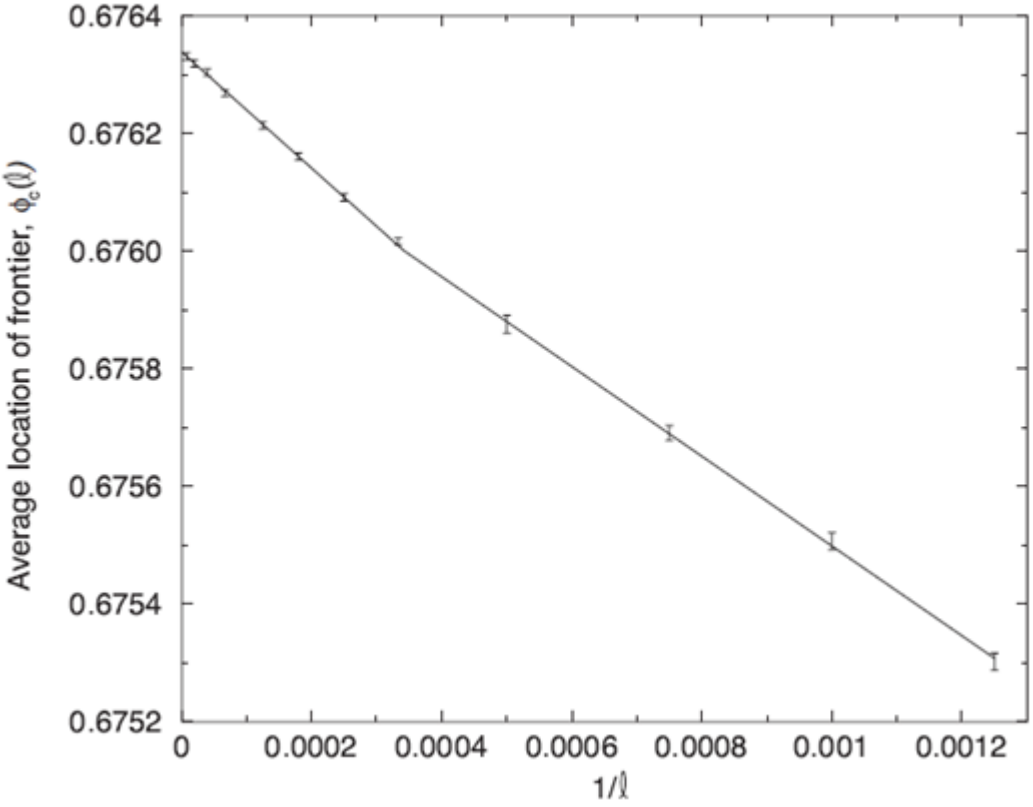

Figure.4-4 The average location of the frontier $\emptyset_c(l)$

Roberts [13]	0.62
Domb [14]	0.67
Pike and Seager [15]	0.675 (2)
Fremlin [16]	0.667 (2)
Haan and Zwanzig [17]	0.683 (3)
Gawlinski and Stanley [18]	0.676 (2)
Rosso [4]	0.676 6(5)
Lorenz *et al* [19]	0.676 4(9)
Quintanilla and Torquato [1]	0.676 37(5)
Present work	0.676 339(4)

Table 4-1 Estimates of the percolation threshold $\emptyset_c$ for fully penetrable disks

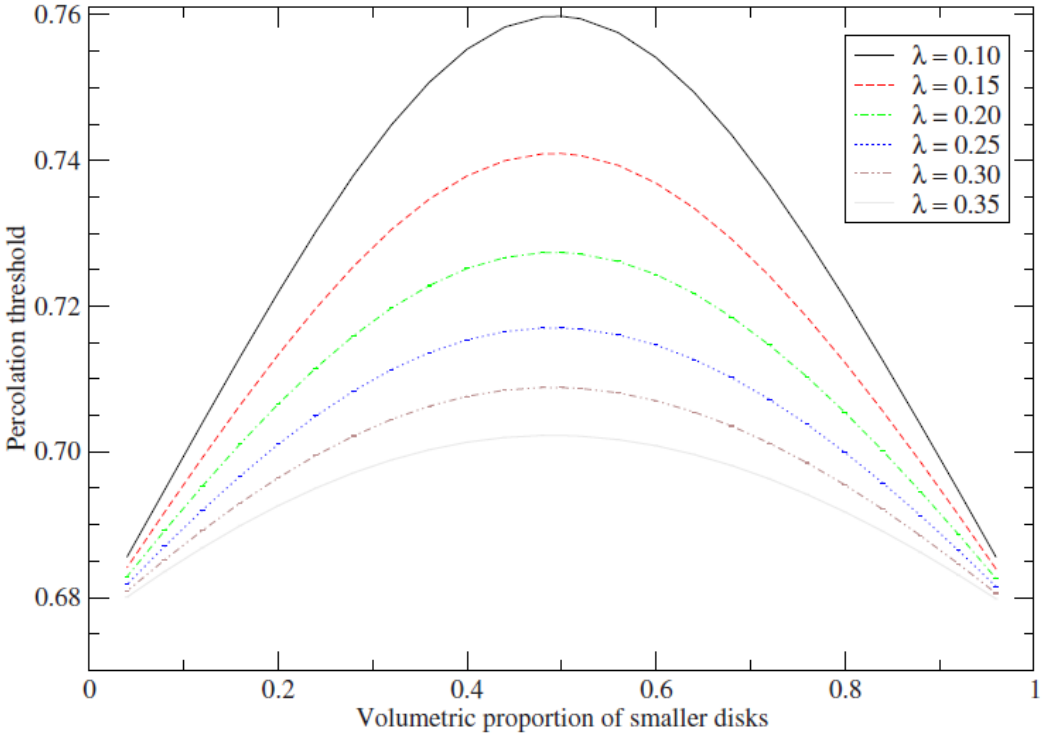

Figure 4-5 Estimates of the percolation threshold $\emptyset_c(v, \lambda)$ for , $0.1 \leq \lambda \leq 0.35$.

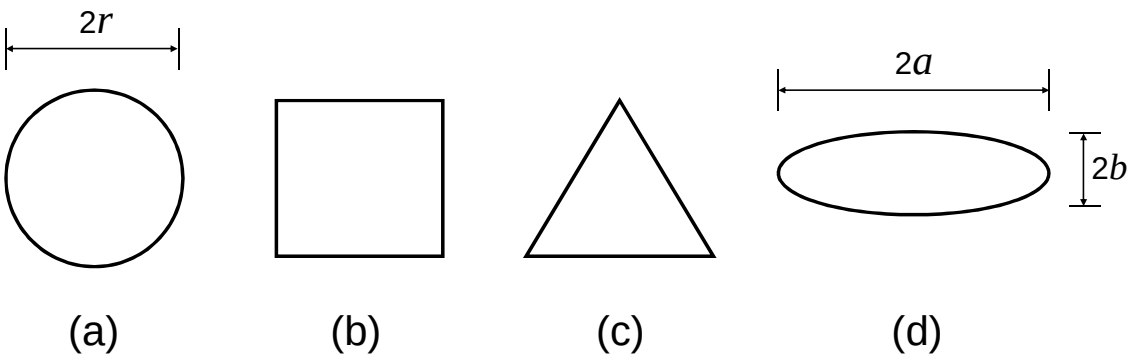

Figure 4-6 Four fundamental geometries of disks under investigation.

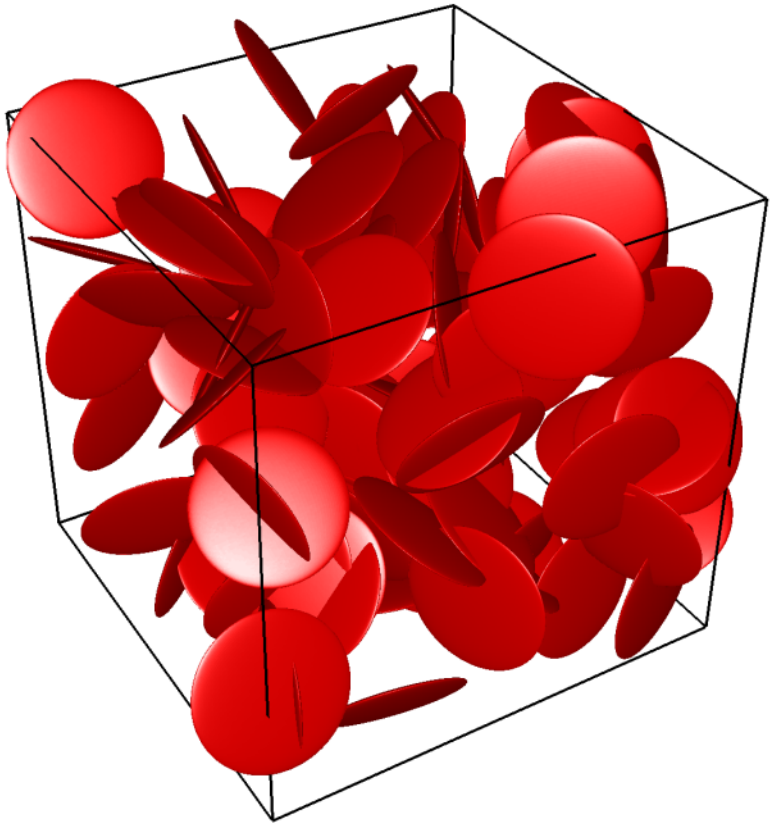

Figure 4-7 Computer realization of 100 random disks of circular shape in 3-D.

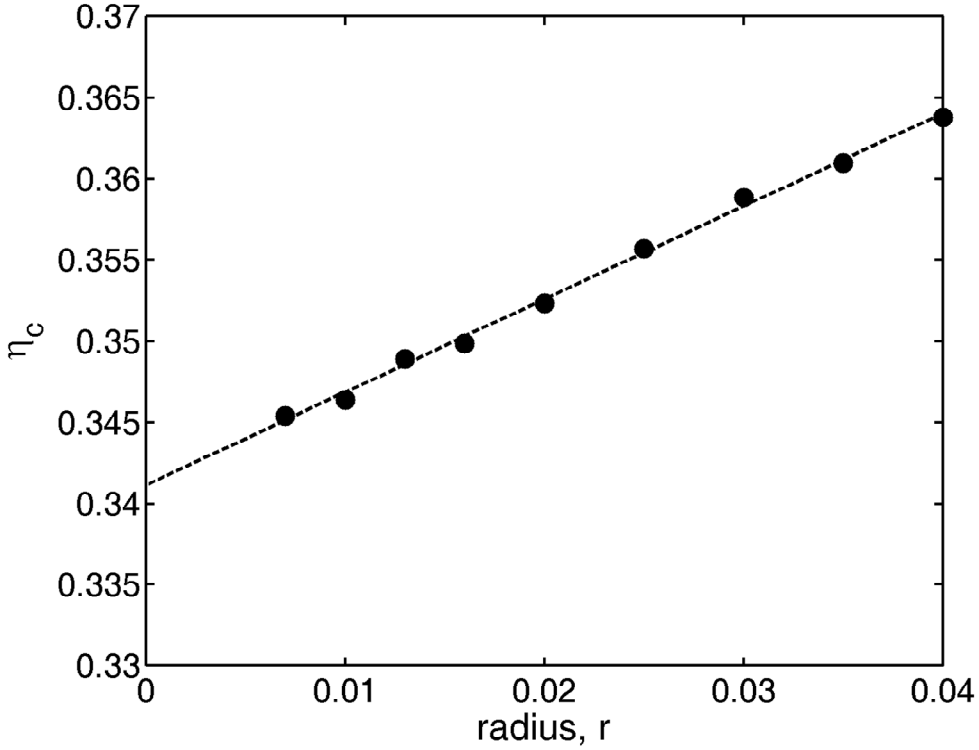

Figure 4-8 Determination of percolation threshold for spheres.

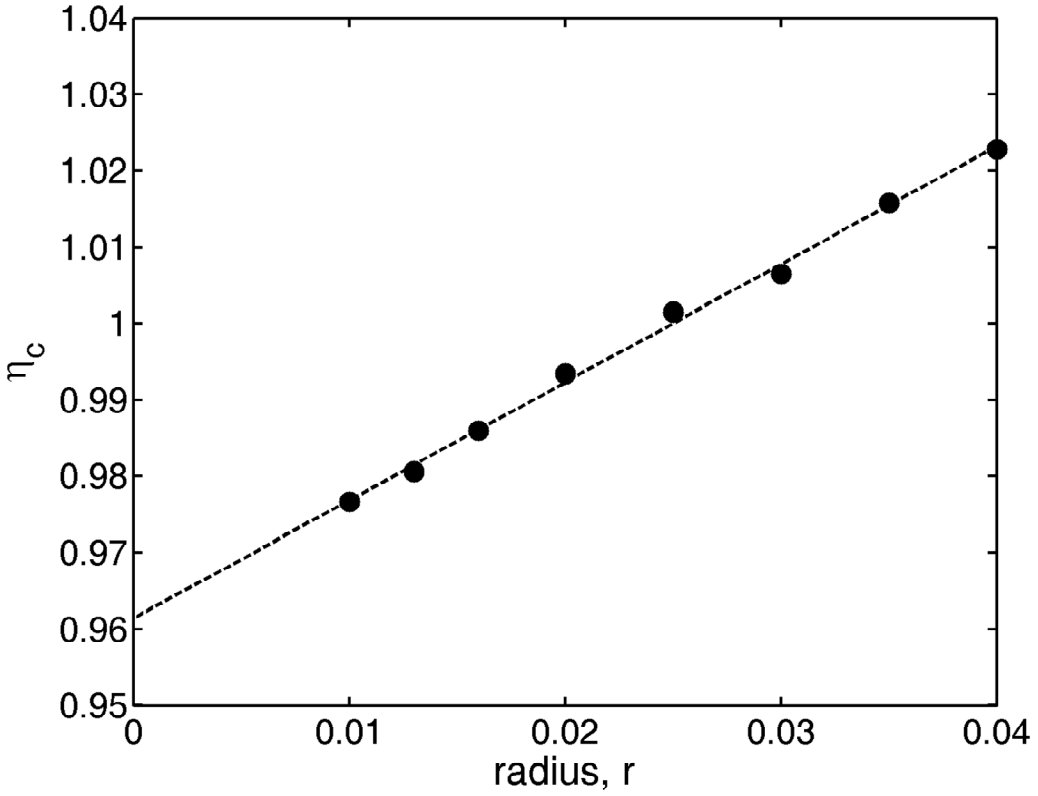

Figure 4-9 Determination of percolation threshold for circular disks in 3-D.

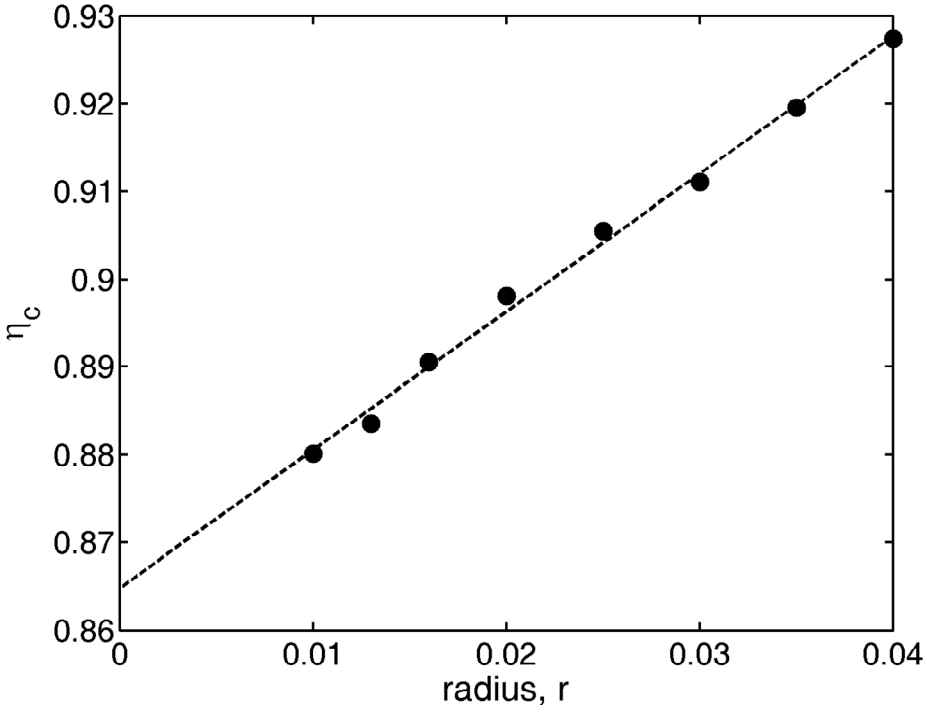

Figure 4-10 Determination of percolation threshold for square disks in 3-D.

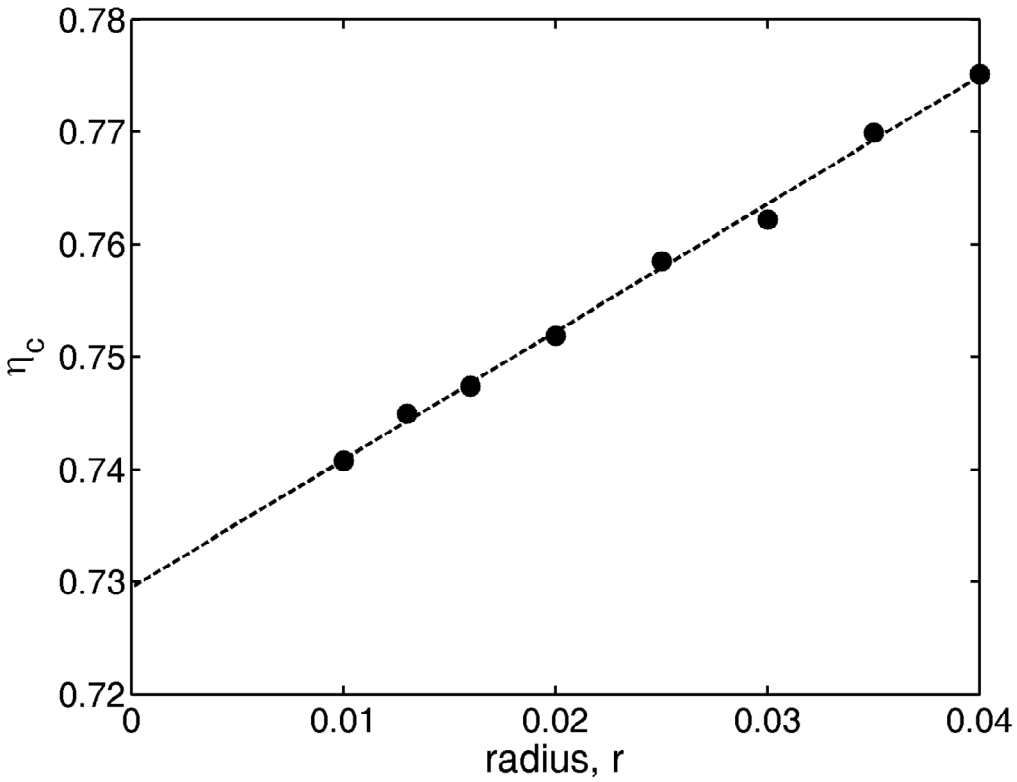

Figure 4-11 Determination of percolation threshold for triangular disks in 3-D.

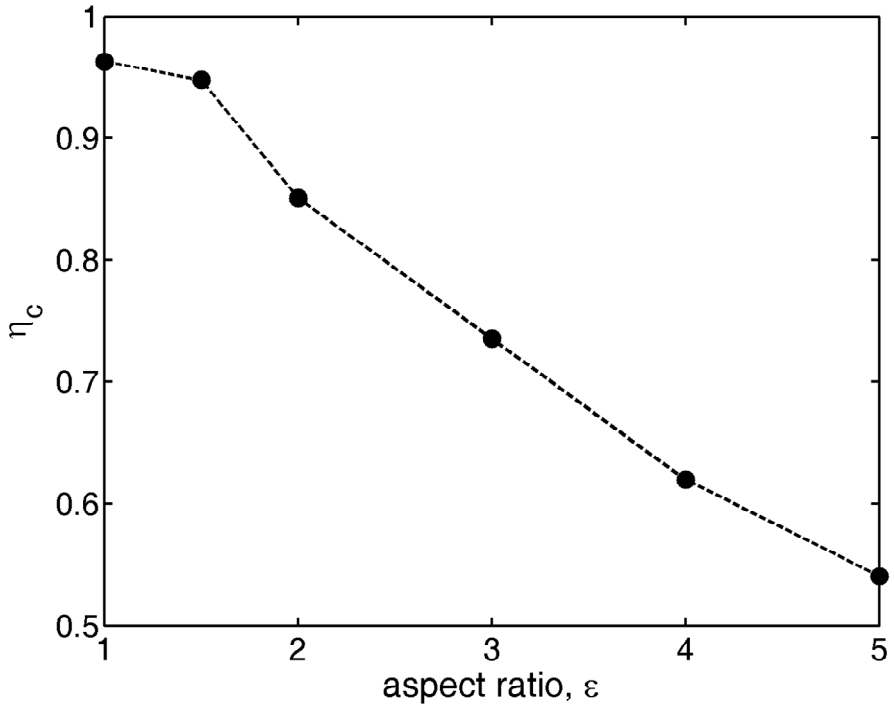

Figure 4-12 Percolation threshold as a function of the aspect ratio of elliptical disks in 3-D.

Table 4-2 Estimates of the percolation thresholds for different geometries in 3-D

	spheres	circular plates	square plates	triangular plates
η_c	0.3412	0.9614	0.8647	0.7295
error	±0.0003	±0.0005	±0.0006	±0.0006

Table 4-3 Estimates of the percolation thresholds for binary dispersion of circular plates in 3-D

λ	0.1	0.2	0.3	0.4	0.5	0.6	0.7	0.8	0.9
η_c	0.9612	0.9688	0.9734	0.9756	0.9815	0.9788	0.9703	0.9640	0.9616
error	±0.0007	±0.0005	±0.0007	±0.0006	±0.0005	±0.0007	±0.0004	±0.0006	±0.0006

CHAPTER 5 CONCLUSIONS AND FUTURE WORK

5.1 Effective Properties of Two-phase Media

In this work, a finite element modeling approach was successfully implemented to investigate the elastic modulus and conductivity of heterogeneous composites containing particulate inclusions. Both 2-D and 3-D models were developed and the simulation results were compared to the existing analytical approximation theories. Several important conclusions can be drawn from this study:

(1) Randomness in the particle distribution has an impact on the properties of a two-phase particulate material system. For solid inclusions, the effective medium theories are capable of predicting the material properties quite well, but the predictions on void inclusions are much less reliable.

(2) Among the various approximation methods, the SC solution yields much better results than the other methods including the Maxwell solution, the DEM solution and the rules of mixing. However, the SC approximation is less accurate in the following two situations: (a) particulate inclusions of large aspect ratios, and (b) soft inclusion material (namely, the modulus of the matrix is higher than that of the inclusions).

(3) Both the effective elastic modulus and conductivity show relatively weak dependence on the permeability of the particulate inclusions- that is, at the same

volume fraction, the overlapping particles and nonoverlapping particles almost yield the same results.

(4) Investigation of the morphological shape of the inclusions reveals that at higher volume fractions, the prolate particles yield a higher elastic modulus and a higher conductivity than the oblate particles. However their differences are not significant.

(5) There is no monotonic relationship between the properties of material containing ellipsoidal inclusions and the particle aspect ratio. The exact locations of the maxima depend on the properties of both material phases.

It should be pointed out that the 3-D models and methodologies developed in this paper may provide a convenient way to study mechanical and transport properties of multiphase composites for not only spherical and ellipsoidal inclusions, but also short fibers and filler contents of other shapes.

5.2 Geometric percolation thresholds of plates in three-dimensional space

The geometric percolation involving plates in the 3-D space has been studied using a Monte Carlo simulation method. Four different geometries are studied: circles, ellipses, squares and triangles, which represent the geometric limits of oblate particles when one of the axes degenerates to zero. The plate-plate intersection criteria for the four geometries are established analytically. The percolation probability at various equivalent radii is computed and the percolation threshold is estimated at the limit of zero radius by linear extrapolation. An error analysis is successfully applied to estimate the solution

tolerance. Comparisons among different geometries show that the global or local curvatures tend to increase the interparticle connectivity and thus reduce the percolation point. For elliptical plates, the percolation threshold has been found as a monotonic function of the particle aspect ratio, which is consistent with the results for ellipsoids or planar ellipses. When disks of two different radii are mixed together, the percolation threshold does not change significantly, with a peak value located where the ratio of the two radii is approximately 0.5. Some results have also been compared to the data reported in the literature. The results and methods used in the current study are useful in predicting conduction and percolation characteristics of multiphase material systems containing oblate particles of thin thickness.

LIST OF REFERENCES

ABAQUS Standard® 6.5 User's Manual, ABAQUS, Inc.; 2006.

Baker, D., Paul, G., Sreenivasan, S., & Stanley, H. (2002). Continuum percolation threshold for interpenetrating squares and cubes. Physical review E , 66, 046136-1-046136-5.

Berhan, L. , Yi, Y. B. , Sastry, A. M. , Munoz, E. , Selvidge, M. , & Baughman, R. (2004). Mechanical properties of nanotubes sheets Alterations in joint morphology and achievable moduli in manufacturable materials. Journal of Applied Physics, 95 (8), 4335-4345.

Benveniste, Y. A. (2006). General interface model for a three-dimensional curved thin anisotropic interphase between two anisotropic media. *Journal of the Mechanics and Physics of Solids*, 54,708-734.

Bruggeman, D. (1935). Calculation of various physical constants of Heterogeneous substances, *Annalen der Physik*, 24, 636-679.

Budiansky, B. (1965). On the elastic moduli of some heterogeneous materials, *Journal of the Mechanics and Physics of Solids*, 13, 223-227.

Cai, W., Tu, S, & Tao, G. (2005). Thermal conductivity of PTFE composites with three-dimensionalrandomly distributed fillers. *Journal of Thermoplastic Composite Materials* , 18, 241-253.

Chen, J., Xu, L., & Li, H. (2008). Investigationon a direct modeling strategy for the effective elastic moduli prediction of composite material. *Material Science and Engineering A*, 491, 385-389.

Choy, T. C. (1999). Effective Medium Theory. New York: Oxford University Press Inc.

Coniglio, A., Deangelis, U., Forlani, A., & Lauro, G. (1977). Distribution of physical clusters. *Journal of Physics A* ,10, 219-228..

Consiglio, R. , Baker, D. R. , Paul, G. , & Stanely, H. E. (2003). Continuum percolation thresholds for mixtures of spheres of different sizes. *Physica A*, 319, 49-55.

COMSOL Multiphysics ® 3.3 User's Manual, COMSOL, Inc.;2006.

Deutcher, G. (1983). Percolation structures and processes. Inst of Physics pub Inc.

Dhar, D. (1990). Self-organized critical state of sandpile automaton models. Physics Review Letters, 64, 1613-1616.

Dundurs, J. (1969). Discussion on edge bonded dissimilar orthogonal elastic wedges under normal and shear loading. *Journal* of *Applied* Mechanics, 36, 650-652.

Essam, J. W. (1971). The scaling laws for percolation processes. Journal of physics C: Solid state physics , 4, L228.

Floy, P. j. (1941). MOlecular size distibution in three dimensional polymers. Journal of the american chemical society , 63 (11), 3083-3090.

Garboczi, E. J. , Snyder, K. A. , Douglas, J. F. , & Thorpe, M. F. (1995). Geometrical percolation threshold of overlapping ellipsoids. Physics Review, 52, 819-828.

Garboczi, E.J., & Day, A.R. (1995). An algorithm for computing the effective linear elastic properties. J. Mech. Phys. Solids. 43, 1349-1362.

Garboczi, E.J., & Berryman, J.G. (2001). Elastic moduli of a material containing composite inclusions: effective medium theory and finite element computations. *Mechanics of Materials*, 33. 455-470.

Gubernate, J. E., krumbansl, J. A. (1975). Macroscopic engineering properties of polycrystalline materials: Elastic properties. *Journal of Applied Physics*, 46. 1875-1883.

Hashin, Z., Shtrikman, S. (1963). A variational approach to the theory of the elastic behavior of multiphase materials. *Journal of the Mechanics and Physics of Solids*, 11, 127-140.

Hashin, Z. (1983). Analysis of composite materials: A survey. *Journal* of *Applied* Mechanics, 50,48 l-505.

Hill, R. (1965). A self-consisitent mechanics of composite materials. *Journal of the Mechanics and Physics of Solids*, 13, 213-222.

Lee, K. Y., & paul, D. R (2005). A model for composites containing three-dimensional ellipsoidal inclusions. *Polymer*, 46, 9064-9080.

Lorenz, C. D., & Ziff, R. M. (2001). Precise determination of the critical percolation threshold for the three-dimensional "Swiss cheese" model using a growth algorithm. Journal of chemical physics , 14, 3659-3661.

MATLAB® 7.1 User's Manual, MathWorks, Inc.;2005.

Maxwell, J. C. (1873), Treatise on Electricity and Magnetism, Clarendon Press, Oxford.

Mclaughlin, R. (1977).A study of the differential scheme for composite materials. *International Journal of Engineering Science* ,15, 237-244.

Miloh, T., & Benveniste, Y. (1999). On the effective conductivity of composites with ellipsoidal inhomogeneities and highly conducting interfaces. *Proceedings of the Royal Society A: Mathematical, Physical & Engineering Sciences*, 455, 2687-2706.

Mondescu, R., & Muthukumar, M. (1999, January 8). Effective elastic moduli of a composite containing rigid spheres at nondilute concentrations: A. *Journal of Chemical Physics*, 110 (2), 1123.

Mohanty, S. & Sharma, M. (1991). A Monte Carlo RSRG mehtod for the percolation/ conduction properties of correlated lattices. Physics Letter A (154), 475.

Pike, G. E., & Seager, C. H. (1974). Percolation and conductivity: A Computer Study. Physics Review B (10), 1421.

Quintanilla, J. , Torquato, S. , & Ziff, R. M. (2000). Efficient measurement of the percolation threshold for fully penetrable discs. Jouranl of Physics A Math. Gen. (33), L399.

Quintanilla, J. A. , & Ziff, R. M. (2007). Asymmetry in the percolation thresholds of fully penetrable disks with two different radii. Physics Review E (76), art.051115.

Quintanilla, J. (2001). Measurement of the percolation threshold for fully penetrable disks of different radii. Physics Review E (74), art. 031112.

Quintanilla, J., & Torquato, S. (1996). Clustering properties of d-dimensional overlapping spheres. Physics Review E (54), 5331.

Rintoul, M. D., & Torquato, S. (1997). Precise determination of the critical threshold and exponents in a three-dimensional continuum percolation model. Journal of Physics A: Math. Gen. (30), L585.

Roberts, A. P., Garboczi, E. J. (2003). User Manual for Finite Element and Finite Difference Programs: A Parallel Version of NISTIR−6269. Retrieved June 2008, from Virtual Cement and Concrete Testing Laboratory 1.1: http://ciks.cbt.nist.gov/garbocz/nistir6997/

Sahimi, M. (2003). Heterogeneous Materials I. New York: Springer-Verlag new York. Inc.

Stauffer, D. & Aharony, A. (2003). Introduction to percolation theroy. Philadelphia: Taylor & Francis Inc,.

Stephens, R. I., Fatemi, A., Stephens, R. R.,& Fuchs, H. O. (2001). Metal Fatigue in engineering. Jhon Wiley & Sons, Inc.

Stockmayer, W. H. (1943). Theory of molecular size distribution and gel formation in branched-chain polymers. Journal of chemical physics , 11 (2), 45.

The Mathworks. (2008). Retrieved June 6, 2008, from Matlab Function Reference: http://www.mathworks.com.

Torquato, S. (1991). Random heterogeneous media: Microstructure and improved bounds on the effective properties, Appl, Mech. Rev. 44, 37-76.

Torquato, S. (2002). Random Heterogeneous Materials. New York: Springer Science & Business Media.

Torquato, S. , & Rintoul, M. D. (1995). Effect of the interface on the properties of composite media. Phys Rev Lett;75:4067-70.

Wei, C. & Srivastava, D. (2004). Structural ordering in nanotube polymer composites. Nano Letters , 4 (10), 1949-1952.

W. Chenyu & S. Deepak (2004). Structural Ordering in Nanotube Polymer Composites. Nano Lett. 4. 1949-1952.

Wang CW, Yi YB, Sastry AM. Particle compression and conductivity in Li-ion anodes with graphite additives. J Electrochemical Society 2004;151:A1489-98.

Xia, W. , & Thorpe, M. F. (1988). Percolation properties of random ellipses. Physics Review A (38), 2650.

Yi, Y. B. , & Sastry, A. M. (2002). Analytical approximation of two-dimensional percolation threshold for fields of overlapping ellipses. Physics Review E (66), art. 066130.

Yi, Y. B., & Sastry, A. M. (2004). Analytical approximation of the percolation threshold for overlapping ellipsoids of revolution. Proceedings of the Royal Society A. 460, 2353-2380.

Yi, Y. B. , Wang, C. W. , & Sastry, A. M. (2004). Two-dimensional vs three-dimensional clustering and percolation fields of overlapping ellipsoids. Journal of Electrochemical Society (151), A1292.

Yi, Y. B. (2008). The role of interparticle in conductive properties of random particulate materials. Acta Materialia (56), 2810.

Yi, Y. B. (2006). Void percolation and conduction of overlapping ellipsoids. Physics Review E (74), art. 031112.

Yi, Y.B., Sastry, A. M.(2006). Analytical approximation of the percolation threshold for overlapping ellipsoids of revolution. Pro R Soc Lond A 2004;460:2353-80.
Yi, Y.B.(2007).. Void percolation and conduction of overlapping ellipsoids. Phys Rev E 2006;74:art 031112.

Zhang T, Yi YB. Monte Carlo simulations of effective electrical conductivity in short-fiber composites. J Appl Phys 2008;103:art 014910.